Statistics of Chaotic Impedance and Scattering Matrices:
The Random Coupling Model

Xing Zheng, Thomas M. Antonsen Jr.,[*] and Edward Ott[*]

Department of Physics

and Institute for Research in Electronics and Applied Physics,

University of Maryland,

College Park, MD, 20742

(Dated: January 28, 2004)

We propose a model to study the statistical properties of the impedance (Z) and scattering (S) matrices of open electromagnetic cavities with several transmission lines or waveguides connected to the cavity. The model is based on assumed properties of chaotic eigenfunctions for the closed system. Analysis of the model successfully reproduces features of the random matrix model believed to be universal, while at the same time incorporating features which are specific to individual systems. Statistical properties of the cavity impedance Z are obtained in terms of the radiation impedance (i.e., the impedance seen at a port with the cavity walls moved to infinity). Effects of wall absorption and nonreciprocal media (e.g., magnetized ferrite) are discussed. Theoretical predictions are tested by direct comparison with numerical solutions for a specific system.

Keywords: wave chaos, impedance, scattering matrix

I.   INTRODUCTION

The problem of the coupling of electromagnetic radiation in and out of structures is a general one which finds applications in a variety of scientific and engineering contexts. Examples include the susceptibility of circuits to electromagnetic interference, the confinement of radiation to enclosures, as well as the coupling of radiation to accelerating structures.

Because of the wave nature of radiation, the coupling properties of a structure depend in detail on the size and shape of the structure, as well as the frequency of the radiation. In considerations of irregularly shaped electromagnetic enclosures for which the wavelength is fairly small compared with the size of the enclosure, it is typical that the electromagnetic field pattern within the enclosure, as well as the response to external inputs, can be very sensitive to small changes in frequency

---

[*]Also at Department of Electrical and Computer Engineering.

and to small changes in the configuration. Thus, knowledge of the response of one configuration of the enclosure may not be useful in predicting that of a nearly identical enclosure. This motivates a statistical approach to the electromagnetic problem.

There are many examples of situations in which a statistical description is called for. It may be that many devices are manufactured, and, while nearly identical, they may have small differences. These small differences may lead to large fluctuations in appropriate wave quantities. In such a case, the statistics, as characterized by the probability distribution function of the appropriate wave quantity, is of interest. As another example, a specific single device may be intended to operate in some frequency range, and, within this range, there may be extremely rapid, complicated variation of an electromagnetic quantity of interest. Furthermore, it may be that, on different occasions the device is operated at different frequencies within the allowed range. In this case it is of interest to know the probability distribution function of the relevant electromagnetic quantity for a randomly chosen value of frequency in the allowed range. As still another example, an enclosure may have within it flexible cables whose placement is occasionally changed, critically affecting the detailed field distribution within the enclosure and its responses at its ports.

While our ability to numerically compute the response of particular structures has advanced greatly in recent years, the kind of information needed for a statistical description may not be obtainable directly from numerical computation. In the case of complex or irregularly shaped enclosures that are large compared to a wavelength, accurate numerical solution of the electromagnetic field problem can be difficult or impossible. Also, if such numerical solutions are to be used to generate statistics, the numerical solutions must be obtained for many slightly different configurations and/or frequencies.

Thus it would seem to be desirable to have specific analytical predictions for the statistics of electromagnetic quantities in such circumstances. This general problem has received much attention in previous works (e.g., Refs. [1–7]). Some of the main issues addressed in these works are: the probability distribution of fields at a point, the correlation function of fields at two points near each other, the statistics of the excitation of currents in cables or in small devices within the enclosure, the cavity Q, the statistics of coupling to the enclosure, and the statistics of scattering properties. A fundamental basis for most of these studies is that, due to the complexity of the enclosure and the smallness of the wavelength compared to the enclosure size, the electromagnetic fields approximately obey a statistical condition that we shall call *the random plane wave hypothesis.* According to this hypothesis, the fields in any small region within the interior of the enclosure are, in some suitable sense, similar to what would result from a spatially uniform random superposition

of many plane waves whose polarizations are randomly oriented in the plane perpendicular to the direction of propagation of the plane wave, whose phases are randomly assigned, and whose propagation directions are assigned randomly with an isotropic distribution. This work has been quite successful in obtaining meaningful predictions, and some of these have been tested against experiments with favorable results. A good introduction and overview is provided in the book by Holland and St. John [1].

In addition to this previous work on *statistical electromagnetics* [1–7], much related work has been done by theoretical physicists. The physicists are interested in solutions of quantum mechanical wave equations when the quantum mechanical wavelength is short compared with the size of the object considered. Even though the concern is not electromagnetics, the questions addressed and the results are directly applicable to wave equations, in general, and to electromagnetics, in particular. The start of this line of inquiry was a paper by Eugene Wigner [8]. Wigner's interest was in the energy levels of large nuclei. Since the energy level density at high energy is rather dense, and since the solution of the wave equations for the levels was inaccessible, Wigner proposed to ask statistical questions about the levels. Wigner's results apply directly to the statistics of resonant frequencies in highly-overmoded irregularly-shaped electromagnetic cavities. Since Wigner's work, and especially in recent years, the statistical approach to wave equations has been a very active area in theoretical physics, where the field has been called 'quantum chaos'. We emphasize, however, that the quantum aspect to this work is not inherent, and that a better terminology, emphasizing the generality of the issues addressed, might be 'wave chaos'. For a review see Chapter 11 of Ref. [9] or the books [10, 11].

In this paper we consider an irregularly shaped cavity with transmission lines and/or waveguides connected to it, and we attempt to obtain the statistical properties of the impedance matrix Z and the scattering matrix S characterizing the response of the cavity to excitations from the connected transmission lines and/or waveguides in the case where the wavelength is small compared to the size of the cavity. We will only treat the case of cavities that are thin in the vertical (z-direction) direction. In this case the resonant fields of the closed cavity are transverse electromagnetic (TEM, $\vec{E} = E_z(x,y)\hat{z}$), and the problem admits a purely scalar formulation. While the two dimensional problem has practical interest in appropriate situations (e.g., the high frequency behavior of the power plane of a printed circuit), we emphasize that our results for the statistical properties of Z and S matrices are predicted to apply equally well to three dimensional electromagnetics and polarized waves. We note that previous work on statistical electromagnetics [1–7] is for fully three dimensional situations. Our main motivation for restricting our considerations here to two

dimensions is that it makes possible direct numerical tests of our predictions (such numerical predictions might be problematic in three dimensions due to limitations on computer capabilities). Another benefit is that analytical work and notation are simplified.

Our paper is organized as follows. In Sec. II, as background for our work, we review previous relevant developments mostly from the physics literature. Following some preliminaries (Sec. III), Sec. IV presents our statistical model. Section V illustrates our model by application to the statistics of the impedance seen at a single transmission line input to a cavity that is irregularly-shaped, highly over-moded, lossless, and non-gyrotropic (i.e., no magnetized ferrite). Section VI applies the model to obtain the impedance statistics in more general cases, including multiple inputs (in which case the impedance is a matrix rather than the scalar of Sec. IV), gyrotropic media, and losses. Section VII relates the impedance matrix characteristics to those of the scattering matrix. Throughout, our analytical results will be compared with direct numerical solutions of the wave problem. Section VIII concludes with a discussion and summary of results.

II. BACKGROUND

In this section we will review previous work that is relevant to the subsequent discussion in the paper. Most of this review concerns work done in the context of quantum mechanics and can also be found in Refs. [9–11]. For definiteness, when we give examples, it will often be in the context of the two-dimensional Helmholtz equation, $(\nabla^2 + k^2)\phi = 0$, with $\phi = 0$ on the boundaries. This example is relevant to quantum dots [12], which motivates some of the work reviewed below, but it is also clearly relevant to the case of vertically thin electromagnetic cavities.

A. Eigenvalue Statistics

In considering a closed system Weyl [9, 13] gave a result for the approximate average eigenvalue density in the limit of small wavelength compared to the system size. For the two-dimensional problem $(\nabla^2 + k^2)\phi = 0$ in a region R of area A, Weyl's formula reduces to

$$\tilde{\rho}(k^2) \cong A/4\pi \; , \tag{1}$$

where $\tilde{\rho}(k^2)\delta k^2$ is the number of eigenvalues k_n^2 ($k_1^2 \leq k_2^2 \leq k_3^2 \leq \ldots$) between $(k^2 - \delta k^2/2)$ and $(k^2 + \delta k^2/2)$. The quantity

$$\Delta(k^2) = 1/\tilde{\rho}(k^2)$$

4

is the average spacing between eigenvalues [average of $(k_{n+1}^2 - k_n^2)$ for $k_n^2 \cong k^2$]. Inherent in the derivation of (1) are the assumptions that $\delta k^2 \ll k^2$ and that many modes are present in the range δk^2. These imply the requirement that $k^2 A \gg 4\pi$, the previously mentioned small wavelength limit. Higher order corrections to the Weyl formula (e.g., terms of order ℓ/k added to the right hand side of (1), where ℓ is a relevant length of the boundary) have been given in Refs. [14, 15]. Other corrections due to Gutzwiller are oscillatory in k and are geometry dependent [10, 16]. For a three dimensional electromagnetic enclosure Weyl's formula becomes

$$\Delta(k^2) = 1/\tilde{\rho}(k^2) = 2\pi^2/kV,$$

where V is the volume of the enclosure. We note that $\Delta(k^2)$ depends on k in the three dimensional case, but is k-independent in two dimensions. Since we work primarily in two dimensions, we henceforth use the notation Δ in place of $\Delta(k^2)$.

If one examines the spacings between two adjacent eigenvalues, $k_{n+1}^2 - k_n^2$, then, *on average* it is well-approximated by $1/\Delta$ with Δ given by the Weyl formula. However, the fluctuations from the average are themselves typically of order $1/\Delta$. Thus it is of interest to consider the distribution function of the eigenvalue spacings for a random choice of adjacent eigenvalues in the range $(k^2 - \delta k^2/2)$ to $(k^2 + \delta k^2/2)$. As a first step we can normalize the spacings using the Weyl formula,

$$s_n = (k_{n+1}^2 - k_n^2)\Delta . \tag{2}$$

Wigner considered the probability distribution function for the eigenvalues (energy levels) of large complicated nuclei. Depending on symmetries, he found three cases, only two of which are relevant for us. These two cases are referred to as the Gaussian Orthogonal Ensemble (GOE) and the Gaussian Unitary Ensemble (GUE) (to be explained subsequently). Wigner's surmise for the probability distributions $P(s)$ of the normalized spacing (2) are [8–11]

$$P_{GOE}(s) \cong (\pi/2)s \exp(-\pi s^2/4) , \tag{3}$$

and

$$P_{GUE}(s) \cong (32/\pi)s^2 \exp(-4s^2/\pi) . \tag{4}$$

These spacing distributions, while derived for a very specific model, have been found to apply in a variety of contexts, including the spacing distributions for modes of electromagnetic resonators. Other statistical properties of the spectrum can be quantified. These will be discussed in more detail as they are needed.

B.   Random Matrix Theory

We now explain the idea behind Wigner's derivations of (3) and (4), first considering (3) which applies to our example, the eigenvalue problem,

$$(\nabla^2 + k^2)\phi = 0 \quad \text{in} \quad R \ , \tag{5}$$

$$\phi = 0 \quad \text{on the boundary of } R \ , \tag{6}$$

where R is a finite connected two dimensional domain and $\nabla^2 = \partial^2/\partial x^2 + \partial^2/\partial y^2$. Introducing a real orthonormal basis $\psi_j(x,y)$ $(j = 1, 2, \ldots)$, where ψ_j satisfies the boundary condition (6) [note, ψ_j are in general *not* the solutions of the eigenvalue problem (5,6)], we express $\phi(x,y)$ as

$$\phi = \sum_j c_j \psi_j \ . \tag{7}$$

Substituting (7) in (5) multiplying by ψ_i and integrating over R we obtain the infinite matrix problem,

$$Hc = \Lambda c \ , \tag{8}$$

where $\Lambda = -k^2$, $c = (c_1, c_2, \ldots)^T$ (the superscribed T denotes the transpose), and the elements of H are

$$H_{ij} = \int \int_R \psi_i \nabla^2 \psi_j dx dy \ . \tag{9}$$

Note that, aside from the conditions of orthonormality and the satisfaction of the boundary conditions, Eq. (6), the basis functions $\psi_j(x,y)$ are so far arbitrary. Nevertheless, we still know something about the matrix H: It is real, and, via integration of (9) by parts, it is also symmetric. Wigner hypothesized that the eigenvalue spectrum of complicated nuclear systems have similar statistical properties to those of the spectra of ensembles of random matrices. That is, we take the infinite dimensional matrix H in (8) to be randomly drawn from some large collection of matrices (the 'ensemble'). Wigner further hypothesized that the following two statistical conditions on the probability distribution $\bar{P}(H)$ for the ensemble of matrices should be satisfied.

(1) *Invariance*. The probability distribution should be independent of the choice of basis $\{\psi_i\}$. Expressing the eigenvalue problem (8) in another orthonormal basis $\{\psi_i'\}$ transforms the vector of expansion coefficients c to another vector of expansion coefficients c',

$$c' = Oc \ , \tag{10}$$

where O is an orthogonal matrix, $O^T = O^{-1}$. Invariance requires $\bar{P}(H) = \bar{P}(H')$, or

$$\bar{P}(H) = \bar{P}(OHO^T) \tag{11}$$

for all orthogonal matrices O.

(2) *Independence.* The matrix elements (aside from the symmetry $H_{ij} = H_{ji}$) are independent random variables. Thus $\bar{P}(H)$ is the product of distributions for all the individual elements H_{ij}, $i \leq j$ (the value of the element H_{ij}, $i > j$ is implied by the symmetry).

These two conditions can be shown to imply [8–11] that the distributions for the H_{ij} are all Gaussians, that the variances of the off diagonal elements are all the same, and that the variances of all the diagonal element distributions are double the variance of the off diagonal elements. This specifies the Gaussian Orthogonal Ensemble (GOE) of random matrices. Using this distribution for H, Wigner proposed Eq. (3) for the normalized spacing distribution.

Wigner's second result (4) applies to situations in which 'time reversal symmetry is broken'. Most prominently, in the quantum mechanical context, this often occurs as a result of the presence of a magnetic field. To simply see the origin of this terminology, consider the motion of a point charge in a homogeneous magnetic field $B_0 \hat{z}_0$. The motion in the (x, y) plane is circular. If, at any time $t = t_0$, we stop the charge, and reverse its velocity, it does not retrace its path, but, as illustrated in Fig. 1(a), it follows a different circular path. In contrast, the motion of a particle in an arbitrary potential does retrace its path upon reversal of its velocity vector, if there is no magnetic field. The impact of this is that the quantum mechanical wave equation becomes complex; that is, unlike (5), (6), there are imaginary terms present, and these typically cannot be removed by a change of variables. Thus, expanding as before, H is now a complex Hermitian matrix, $H_{ij} = H_{ji}^*$, and (11) is replaced by

$$\bar{P}(H) = \bar{P}(UHU^\dagger) \ , \tag{12}$$

where U is an arbitrary unitary matrix, $U^{-1} = U^\dagger$, with $\dagger$ standing for the conjugate transpose of the matrix. Application of (12) and the independence hypothesis, then leads to the Gaussian Unitary Ensemble (GUE) of random matrices: $Re(H_{ij}) = Re(H_{ji})$; $Im(H_{ij}) = -Im(H_{ij})$; $Im(H_{ii}) = 0$; for $i \neq j$ the random variables $Re(H_{ij})$ and $Im(H_{ij})$ are independent and have equal variance that is the same for all $i \neq j$; for $i = j$ (diagonal terms) all the H_{ii} have equal variance that is twice that of either $Re(H_{ij})$ or $Im(H_{ij})$ for $i \neq j$. The statistics for the normalized eigenvalue spacings in the GUE case is given by (4).

The GUE statistics are also relevant to electromagnetics [17]. In particular, if a lossless magnetized ferrite is present, the basic wave equation becomes complex because the magnetic permittivity
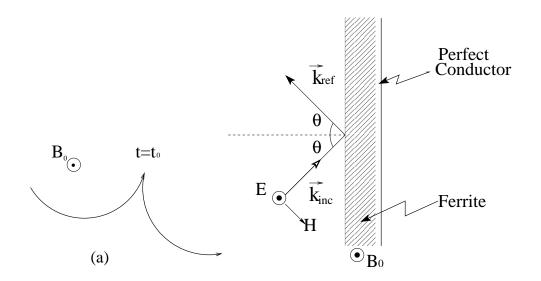
FIG. 1: Time reversal symmetry braking (a) for a particle trajectory in a magnetic field, and (b) for reflection from a lossless magnetized ferrite slab.

matrix μ is Hermitian, $\mu = \mu^\dagger$, with complex off-diagonal elements. As an example of the breaking of 'time reversal symmetry' in the case of a magnetized ferrite, consider Fig. 1(b) which shows a homogeneous lossless ferrite slab, with vacuum in the region to its left, a perfectly conducting surface bounding it on its right, a constant applied magnetic field $B_0 \hat{z}_0$, and a time harmonic electromagnetic plane wave incident on the slab from the left where the angle of incidence is θ. The resulting reflection coefficient for the situation in Fig. 1(b) has magnitude one due to energy conservation, and is thus given by the phase shift $\alpha(\theta, B_0)$ upon reflection. If we now reverse the arrows in Fig. 1(b), the phase shift is different from what it previously was if $B_0 \neq 0$, but is the same if $B_0 = 0$. Thus here too a magnetic field may be said to break time reversal symmetry.

The study of random ensembles of matrices, particularly the GOE and GUE ensembles initiated by the work of Wigner, has become a very highly developed field [18, 19]. Using these ensembles many questions, other than that of finding $P(s)$, have been addressed. We will come back to this later in the paper.

C. Wave Chaos

Wigner's original setting was a very complicated wave system, and it was this complication that he invoked to justify the validity of a statistical hypothesis. Subsequently it was proposed [20, 21] that, under appropriate conditions, even apparently simple systems might satisfy the Wigner hypotheses. The idea was that, since the wavelength is short, the ray equations should

indicate the character of solutions of the wave equation. Considering the example of a vacuum-filled two dimensional cavity (i.e., it is thin in z), the ray equations are the same as those for the trajectory of a point particle: straight lines with specular reflection (i.e., angle of incidence equals angle of reflection) at the boundaries. Such systems are called 'billiards' and have been studied since the time of Birkhoff [22] as a paradigm of particle motion in Hamiltonian mechanics. It is found that typically three different types of motion are possible: (a) integrable, (b) chaotic, and (c) mixed. Whether (a), (b) or (c) applies depends on the shape of the boundary. It is noteworthy that even rather simple boundaries can give chaotic behavior. Thinking of chaotic behavior as complicated, the authors of Refs. [20, 21] proposed that Wigner's hypotheses might apply in situations where the system was simple but the dynamics was chaotic (complicated), and they tested this proposal numerically on systems of the type (5), (6), obtaining results in good agreement with the predicted $P_{GOE}(s)$, Eq. (3). In addition, subsequent experimental [17, 23, 24] work in electromagnetic cavities, both with and without magnetized ferrite, support (3) and (4).

Figure 2 gives some examples of billiard (or cavity) shapes. The rectangle of Fig. 2(a) is an example of an integrable system; particle orbits *separately* conserve the kinetic energies associated with their motion in the x-direction and in the y-direction. On the other hand, this is not true for the examples of chaotic billiard (cavity) shapes shown in Figs. 2(b-e). For these chaotic shapes, the following situation applies. Suppose we pick an initial condition for the particle orbit at random by first choosing a point within the billiard with uniform probability density per unit area and by next choosing an angle θ with uniform probability in 0 to 2π. We then launch the particle with speed v from the chosen point and in a direction θ to the horizontal. With probability one, the resulting orbit will fill the cavity uniformly and isotropically. That is, if one considers a subregion of area A' of the billiard (total area A), and an orbit of length tending to infinity, then (i) the fraction of the total orbit length within the subregion approaches A'/A, and (ii) the orbit orientation angles, weighted by the orbit length within the subregion, approach a uniform distribution in $[0, 2\pi]$. Of course, there are special orbits (e.g., the dashed lines in Figs. 2(c) and (d)) for which (i) and (ii) above are violated, but, if initial conditions are chosen randomly in the manner we have indicated above, then the probability of picking such orbits is zero).

Thus one qualitative difference between the billiard orbits from randomly chosen initial conditions for an integrable case, like Fig. 2(a), as opposed to chaotic cases, like Figs. 2(b-e), is that the velocity direction samples all orientations equally at all spatial points in the chaotic case, but not in the integrable case. Another, perhaps more fundamental, difference is that, if we start two initial conditions at the same (or slightly different) location and with the same speed, but with
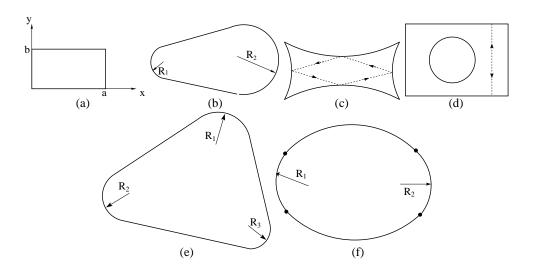
9

FIG. 2: Examples of billiard shapes. (a) Is a rectangle. (b) Is made up of two circular arcs of radii R_1 and R_2 that are tangent at the point of joining to two straight line segments. The sides of (c) are circular arcs. The billiard region of (d) lies between the circle and the square. (e) Is similar to (b). (f) Is made up of four circular arcs that join smoothly at the dots indicated on the boundary; the centers of the upper and lower arcs lie outside the billiard region while the other two arcs of radii R_1 and R_2 have centers that are within the billiard region. (a) Is integrable, (b)-(e) are chaotic, and (f) is mixed.

slightly different angular orientations of their velocity vectors, then the character of the subsequent evolutions of the two orbits is different in the integrable and chaotic cases. In both cases, the two orbits typically separate from each other, but in the integrable case the separation is, on average, proportional to time, while in the chaotic case it is, on average, exponential with time. This exponential sensitivity of randomly chosen orbits to small perturbations is often used as the definition of chaos [9]. Finally, we note that, for the example of Fig. 2(f), there are volumes of the (x, y, θ) phase space for which nearby orbits separate exponentially with time (chaos), interspersed with volumes for which nearby orbits separate linearly with time. Such cases are commonly referred to as 'mixed'. Our interest in this paper is in shapes corresponding to chaos, e.g., Figs. 2(b-e).

Complicated enclosures, possibly containing dielectric objects, small scatters (like bolts or wires), etc., are of great practical interest, perhaps more so than a simple chaotic shape, like one of those in Figs. 2(b-e). In this paper we will, nevertheless, concentrate on a simple cavity of chaotic shape (in particular, Fig. 2(c)). One reason for this choice is that the case of simple cavities of chaotic shape is much more accessible to numerical solution than is the case for complicated configurations, and we will be relying on numerical solutions to validate and test our analytic results. It is our hope that validation in the case of simple two dimensional chaotic cavities implies applicability of our approach to complicated configurations, including three dimensional situations.

D.   The Random Plane Wave Hypothesis

As mentioned in Sec. I, the basis for much of the previous work on statistical electromagnetics [1–7] is 'the random plane wave hypothesis' that, in a suitable approximate sense, the fields within the cavity behavior like a random superposition of isotropically propagating plane waves. The same hypothesis has also been used for waves in plasmas [25] and within the context of quantum mechanics of classically chaotic systems [26]. A strong motivation for this hypothesis is the observation that ray orbits in chaotic systems (like the billiards in Figs. 2(b-e)) are uniform in space and isotropic in direction. Furthermore, direct numerical tests in two dimensional chaotic cavities tend to support the hypothesis [20].

We also note that different predictions result from the random plane wave hypothesis in the cases of time reversal symmetry (i.e., real waves) and of broken time reversal symmetry (i.e., complex waves), and these have been tested in microwave cavity experiments with and without magnetized ferrites [27]. We discuss the case of broken time reversal symmetry further in Sec. VI.B.

In our subsequent work in this paper, we mainly employ the random plane wave hypothesis, although use will occasionally also be made of random matrix theory (in particular, we will use Eqs. (3) and (4)). As will become evident, the random matrix hypotheses of Wigner are closely related to the random plane wave hypothesis. Because the random plane wave hypothesis has a somewhat closer connection to the physical aspects of the problem, it allows a more transparent means of taking into account the nonuniversal effects of the port geometry.

While the random plane wave hypothesis is mostly confirmed by numerical tests, it is also observed that it is sometimes violated. In particular, when many eigenmodes of a very highly overmoded, two-dimensional cavity are computed and examined, it is found, for most modes, that the energy density is fairly uniformly distributed in space over length scales larger than a wavelength [20, 28]. This is in accord with the random plane wave hypothesis. On the other hand, it is also found [28–31] that there is some small fraction of modes for which energy density is observed to be abnormally large along unstable periodic orbits. For example, for a cavity shaped as in Fig. 2(c), a short wavelength mode has been found [31] for which there is enhanced energy density in the vicinity of the dashed, diamond-shaped orbit shown in Fig. 2(c). This phenomenon has been called 'scarring' [28]. One conjecture is that, as the wavelength becomes smaller compared to the cavity size, scarring becomes less and less significant, occurring on a smaller and smaller fraction of modes and with smaller energy density enhancement near the associated periodic orbit [31]. In our work to follow, we will neglect the possibility of scarring. We also note that the scar phenomenon is not

included in the random matrix theory approach.

III. PRELIMINARIES

For an electrical circuit or electromagnetic cavity with ports, the scattering matrix is related to the impedance matrix Z. The impedance matrix provides a characterization of the structure in terms of the linear relation between the voltages and currents at all ports (for a cavity with a waveguide port, the concepts of voltages and currents can be appropriately generalized to describe the waveguide modes),

$$\hat{V} = Z\hat{I}, \tag{13}$$

where $\hat{V}$ and $\hat{I}$ are column vectors of the complex phasor amplitudes of the sinusoidal port voltages and currents. Specifically, the temporally sinusoidally varying voltage $V(t)$ is given in terms of its phasor representation $\hat{V}$ by $V(t) = Re(\hat{V}e^{j\omega t})$.

In defining the S matrix in terms of the Z matrix, we introduce column vectors of incident ($\hat{a}$) and reflected ($\hat{b}$) wave amplitudes,

$$\begin{cases} \hat{a} = (Z_0^{-1/2}\hat{V} + Z_0^{1/2}\hat{I})/2 \\ \hat{b} = (Z_0^{-1/2}\hat{V} - Z_0^{1/2}\hat{I})/2, \end{cases} \tag{14}$$

where Z_0 is a real diagonal matrix whose elements are the characteristic impedances of the transmission line (or wave guide) modes connected to each port. With this definition, the time averaged power delivered to the structure is

$$P = \frac{1}{2}Re\{\hat{I}^\dagger\hat{V}\} = \frac{1}{2}(\hat{a}^\dagger\hat{a} - \hat{b}^\dagger\hat{b}), \tag{15}$$

where $\hat{I}^\dagger = (\hat{I}^T)^*$, $\hat{I}^T$ is the transpose of $\hat{I}$, and $*$ denotes complex conjugate.

The scattering matrix S gives the reflected waves in terms of the incident waves,

$$\hat{b} = S\hat{a},$$

and is related to the impedance matrix Z by substituting

$$\hat{V} = Z_0^{1/2}(\hat{a} + \hat{b}) \quad \text{and} \quad \hat{I} = Z_0^{-1/2}(\hat{a} - \hat{b})$$

into Eq. (13),

$$S = Z_0^{1/2}(Z + Z_0)^{-1}(Z - Z_0)Z_0^{-1/2}. \tag{16}$$

If the structure is lossless, then $Z^{\dagger} = -Z$, S is unitary ($S^{-1} = S^{\dagger}$), and $P=0$.

As discussed in the next section, the impedance matrix Z can be expressed in terms of the eigenfunctions and eigenvalues of the closed cavity. We will argue that the elements of the Z matrix can be represented as combinations of random variables with statistics based on the random plane wave hypothesis for the representation of chaotic wave functions and the Wigner results [3, 4] for the spacing distribution of the eigenvalues.

This approach to determination of the statistical properties of the Z and S matrices allows one to include the generic properties of these matrices, as would be predicted by representing the system as a random matrix from either the Gaussian Orthogonal Ensemble (GOE) or Gaussian Unitary Ensemble (GUE). It also, however, allows one to treat aspects of the S and Z matrices which are specific to the problems under consideration (i.e., so-called *non-universal* properties) and which are not treated by random matrix theory. For example, the diagonal components of the Z matrix have a mean frequency dependent part which strongly affects the properties of the S matrix and depends on the specific geometry of the ports.

The Z matrix also has a fluctuating part. The mean and the fluctuating parts of Z can be directly related to the real and imaginary parts of the complex impedance associated with the same coupling structure radiating into infinite space (i.e., the 'radiation impedance').

IV.   THE RANDOM COUPLING MODEL

We consider a closed cavity with ports connected to it. For specificity, in our numerical work, we consider the particular, but representative, example of the vertically thin cavity shown in Fig. 3(a) coupled to the outside via a coaxial transmission cable. Fig. 3(b) shows an example of how this cavity might be connected to a transmission line via a hole in the bottom plate. The cavity shape in Fig. 3 is of interest here because the concave curvature of the walls insures that typical ray trajectories in the cavity are chaotic. (Fig. 3(a) is a quarter of the billiard shown in Fig. 2(c).) In such a case we assume that the previously mentioned hypotheses regarding eigenfunctions and eigenvalue distributions provide a useful basis for deducing the statistical properties of the Z and S matrices, and, in what follows, we investigate and test the consequences of this assumption. We call our approach the *Random Coupling Model*.

The vertical height h of the cavity is small, so that, for frequencies of interest, only the transverse electric-magnetic (TEM) wave propagates inside the cavity. Thus, the solution for the electric field
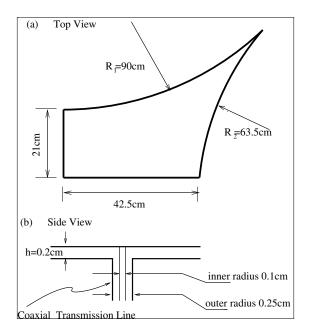
FIG. 3: (a) Top view of the cavity used in our numerical simulation. (b) Side view of the details of a possible coupling.

is of the form:

$$\vec{E} = E_z(x, y)\hat{z}. \tag{17}$$

This electric field gives rise to a charge density on the top plate $\rho_s = -\epsilon_0 E_z$, and also generates a voltage $V_T(x, y) = -hE_z(x, y)$ between the plates. The magnetic field is perpendicular to $\hat{z}$,

$$\vec{B} = (B_x, B_y) = \mu_0 \vec{H}, \tag{18}$$

and is associated with a surface current density $\vec{J}_s = \vec{H} \times \hat{z}$ flowing on the top plate.

The cavity excitation problem for a geometry like that in Fig. 3(b) is system specific. We will be interested in separating out statistical properties that are independent of the coupling geometry and have a universal (i.e., system-independent) character. For this purpose, we claim that it suffices to consider a simple solvable excitation problem, and then generalize to more complicated cases, such as the coupling geometry in Fig. 3(b). Thus we consider the closed cavity (i.e., with no losses or added metal), with localized current sources resulting in a current density $\vec{J}_s(x, y, t) = \sum_i I_i(t)u_i(x, y)\hat{z}$ between the plates. The profile functions $u_i(x, y)$ are assumed to be localized; i.e., $u_i(x, y)$ is essentially zero for $(x - x_i)^2 + (y - y_i)^2 > l_i^2$, where l_i is much smaller than the lateral cavity dimension. $u_i(x, y)$ characterizes the distribution of vertical current at the location of the i-th model input (analogous to the i-th transmission line connected to the cavity).

14

The profile is normalized such that

$$\int dx dy u_i(x, y) = 1. \tag{19}$$

For the sake of simplicity, consider the case in which the cavity is excited by only one input. The injection of current serves as a source in the continuity equation for surface charge, $\partial \rho_s / \partial t + \nabla \cdot \vec{J}_s = Iu(x, y)$, where $\nabla = (\partial / \partial x, \partial / \partial y)$. Expressed in terms of fields, the continuity equation becomes:

$$\frac{\partial}{\partial t}(-\epsilon_0 E_z) + \nabla \cdot (\tilde{H} \times \hat{z}) = Iu(x, y). \tag{20}$$

Differentiating Eq. (20) with respect to t and using Faraday's law, we obtain,

$$\frac{\partial^2}{\partial t^2}(-\epsilon_0 E_z) + \nabla \cdot \frac{1}{\mu_0} \nabla E_z = u(x, y)\frac{\partial I}{\partial t}. \tag{21}$$

Expressing the electric field in terms of the voltage $V_T = -E_z h$, we arrive at the driven wave equation,

$$\frac{1}{c^2}\frac{\partial^2}{\partial t^2}V_T - \nabla^2 V_T = h\mu_0 u\frac{\partial I}{\partial t}, \tag{22}$$

where c is speed of light, $c^2 = 1/(\mu_0 \epsilon_0)$.

Assuming sinusoidal time dependence $e^{j\omega t}$ for all field quantities, we obtain the following equation relating $\hat{V}_T$ and $\hat{I}$, the phasor amplitudes of the voltage between the plates and the port current,

$$(\nabla^2 + k^2)\hat{V}_T = -j\omega h\mu_0 u\hat{I} = -jkh\eta_0 u\hat{I}, \tag{23}$$

where $\eta_0 = \sqrt{\mu_0/\epsilon_0}$ is the characteristic impedance of free space and $k = \omega/c$. Thus Eq. (23) represents a wave equation for the voltage between the plates excited by the input current.

To complete our description and arrive at an expression of the form of Eq. (13), we need to determine the port voltage V. We take its definition to be a weighted average of the spatially dependent voltage $V_T(x, y, t)$,

$$V = \int dx dy u(x, y) V_T(x, y, t). \tag{24}$$

It then follows from Eq. (20) that the product IV gives the rate of change of field energy in the cavity, and thus Eq. (24) provides a reasonable definition of port voltage. Solution of Eq. (23) and application of (24) to the complex phasor amplitude $\hat{V}_T$ provide a linear relation between $\hat{V}$ and $\hat{I}$, which defines the impedance Z.

To solve Eq. (23), we expand $\hat{V}_T$ in the basis of the eigenfunctions of the closed cavity, i.e., $\hat{V}_T = \sum_n c_n \phi_n$, where $(\nabla^2 + k_n^2)\phi_n = 0$, $\int \phi_i \phi_j dx dy = \delta_{ij}$ and $\phi_n(x,y) = 0$ at the cavity boundary. Thus, multiplying Eq. (11) by ϕ_n and integrating over (x,y) yields

$$c_n(k^2 - k_n^2) = -jkh\eta_0\langle u\phi_n\rangle \hat{I}, \tag{25}$$

where $k_n = \omega_n/c$, ω_n is the eigenfrequency associated with ϕ_n, and

$$\langle u\phi_n\rangle = \int \phi_n u \, dx dy.$$

Solving for the coefficients c_n and computing the voltage $\hat{V}$ yields

$$\hat{V} = -j\sum_n \frac{kh\eta_0\langle u\phi_n\rangle^2}{k^2 - k_n^2}\hat{I} = Z\hat{I}. \tag{26}$$

This equation describes the linear relation between the port voltage and the current flowing into the port. Since we have assumed no energy dissipation (e.g., due to wall absorption or radiation), the impedance of the cavity is purely imaginary, as is indicated by Eq. (26).

The expression for Z in Eq. (26) is equivalent to a formulation introduced by Wigner and Eisenbud [32] in nuclear-reaction theory in 1947, which was generalized and reviewed by Lane and Thomas [33], and Mahaux and Weidenmuller [34]. Recently, Fyodorov and Sommers [35] derived a supersymmetry approach to scattering based on this formulation (which they called the "K-matrix" formalism), and it has also been adapted to quantum dots by Jalabert, Stone and Alhassid [36].

Explicit evaluation of Eq. (26) in principle requires determination of the eigenvalues and corresponding eigenfunctions of the closed cavity. We do not propose to do this. Rather, we adopt a statistical approach to the properties of eigenfunctions of chaotic systems, and we use this to construct models for the statistical behavior of the impedance. By a statistical approach we mean the following. For high frequencies such that $k = \omega/c \gg L^{-1}$ where L is a typical dimension of the cavity, the sum in Eq. (26) will be dominated by high order (short wavelength) modes with $k_n L \gg 1$. For these modes the precise values of the eigenvalues k_n as well as the overlap integrals $\langle u\phi_n\rangle$ will depend sensitively on the geometry of the cavity. Rather than predict these values precisely we will replace them with random variables. The assumption here is that there are many modes with k_n in the narrow interval Δk centered at k (where $\Delta \ll \Delta k \ll k$), and, if we choose one of these at random, then its properties can be described by a statistical ensemble. As discussed in Sec. II, the properties of the short wavelength eigenfunctions can be understood in terms of ray trajectories. For geometries like that in Fig. 3(a), ray trajectories are chaotic.

The assumed form of the eigenfunction from the random plane wave hypothesis is

$$\phi_n = \lim_{N \to \infty} \sqrt{\frac{2}{AN}} Re\{\sum_{j=1}^{N} \alpha_j \exp(ik_n \vec{e}_j \cdot \vec{x} + i\theta_j)\}, \tag{27}$$

where $\vec{e}_j$ are randomly oriented unit vectors, θ_j is random in $[0, 2\pi]$, and α_j are random. Using (27) we can calculate the overlap integral $\langle u\phi_n \rangle$ appearing in the numerator of (26). Being the sum of contributions from a large number of random plane waves, the central limit theorem implies that the overlap integral will be a Gaussian random variable with zero mean. The variance of the overlap integral can be obtained using Eq. (27),

$$E\{\langle u\phi_n \rangle^2\} = \frac{1}{A} \int_0^{2\pi} \frac{d\theta}{2\pi} |\bar{u}(\vec{k}_n)|^2, \tag{28}$$

where $E\{.\}$ denotes expect value, and $\bar{u}(\vec{k}_n)$ is the Fourier transform of the profile function $u(x, y)$,

$$\bar{u}(\vec{k}_n) = \int dx dy u(x, y) exp(-i\vec{k}_n \cdot \vec{x}), \tag{29}$$

and $\vec{k}_n = (k_n \cos\theta, k_n \sin\theta)$. The integral in (28) over θ represents averaging over the directions $\vec{e}_j$ of the plane waves.

The variance of $\langle u\phi_n \rangle$ depends on the eigenvalue k_n^2. If we consider a localized source $u(x, y)$ such that the size of the source is less than the typical wavelength $2\pi/k_n$, then the variance will be A^{-1} (recall the normalization of u given by Eq. (19)). As larger values of k_n are considered, the variance ultimately decreases to zero. As an illustrative example, suppose that the source corresponds to an annular ring of current of radius a,

$$u(x, y) = \frac{1}{\pi} \delta(x^2 + y^2 - a^2). \tag{30}$$

In this case, one finds from Eq. (28),

$$E\{\langle u\phi_n \rangle^2\} = A^{-1} J_0^2(k_n a), \tag{31}$$

which decreases to zero with increasing $k_n a$ as $(k_n a)^{-1}$. (A smooth, analytic function $u(x, y)$ will yield a sharper cutoffs in variance as k_n increases.)

Modeling of Eq. (26) also requires specifying the distribution of eigenvalues k_n appearing in the denominator. According to the Weyl formula (1) for a two dimensional cavity of area A, the average separation between adjacent eigenvalues, $k_n^2 - k_{n-1}^2$, is $4\pi A^{-1}$. Thus, one requirement on the sequence of eigenvalues is that they have a mean spacing $4\pi A^{-1}$. The distribution of spacings of adjacent eigenvalues is predicted to have the characteristic Wigner form for cavities with chaotic trajectories. In particular, defining the normalized spacing, $s_n = A(k_n^2 - k_{n-1}^2)/4\pi$, the probability

17

density function for s_n is predicted to be closely approximated by Eq. (3) for chaotic systems with time-reversal symmetry. Thus, a second requirement on the sequence of eigenvalues is that they have the correct spacing distribution. One approach of ours will be to generate values for the impedance assuming that sequences of eigenvalues can be generated from a set of separations s_n which are independent and distributed according to Eq. (3). The usefulness of the assumption of the independence of separations will have to be tested, as it is known that there are long range correlations in the spectrum, even if nearby eigenvalues appear to have independent spacings. A more complete approach would be to use sequence of eigenvalues taken from the spectra of random matrices. We will find that in some cases it is sufficient to consider the simpler spectra, generated from independent spacing distributions, but in other cases, for example, when losses are considered, or when correlations of impedance values at different frequencies are considered, the correlations in eigenvalues exhibited by random matrix theory are important.

A key assumption in our random coupling model is the independence of the overlap integrals, $\langle u\phi_n \rangle$, and the eigenvalues k_n. This we argue on the basis that each eigenfunction satisfies the plane wave hypothesis and successive eigenfunctions appear to be independent. A second justification comes from random matrix theory where it is known that the probability distribution for the eigenvalues of a random matrix is independent of that of the elements of the eigenfunctions [[18], Chap.3].

Combining our expressions for $\langle u\phi_n \rangle$ and using the result that for a two dimensional cavity the mean spacing between adjacent eigenvalues is $\Delta = 4\pi A^{-1}$, the expression for the cavity impedance given in Eq. (26) can be rewritten,

$$Z = -\frac{j}{\pi} \sum_{n=1}^{\infty} \Delta \frac{R_R(k_n)w_n^2}{k^2 - k_n^2}, \tag{32}$$

where w_n is taken to be a Gaussian random variable with zero mean and unit variance, the k_n are distributed independent of the w_n, and R_R is given by

$$R_R(k) = \frac{kh\eta_0}{4} \int \frac{d\theta}{2\pi} |u(\vec{k})|^2. \tag{33}$$

Our rationale for expressing the impedance in the form of Eq. (32) and introducing $R_R(k_n)$ is motivated by the following observation. Suppose we allow the lateral boundaries of the cavity to be moved infinitely far from the port. That is, we consider the port as a 2D free-space radiator. In this case, we solve Eq. (23) with a boundary condition corresponding to outgoing waves, which can be readily done by the introduction of Fourier transforms. This allows us to compute the phasor port voltage $\hat{V}$ by Eq. (24). Introducing a complex radiation impedance $Z_R(k) = \hat{V}/\hat{I}$ (for the

problem with the lateral boundaries removed), we have

$$Z_R(k) = -\frac{j}{\pi} \int_0^\infty \frac{dk_n^2}{k^2 - k_n^2} R_R(k_n), \tag{34}$$

where $R_R(k_n)$ is given by Eq. (33) and k_n is now a continuous variable. The impedance $Z_R(k)$ is complex with a real part obtained by deforming the k_n integration contour to pass above the pole at $k_n = k$. This follows as a consequence of applying the outgoing wave boundary condition, or equivalently, letting k have a small negative imaginary part. Thus, we can identify the quantity $R_R(k)$ in Eq. (33) as the radiation resistance of the port resulting from one half the residue of the integral in (34) at the pole, $k_n^2 = k_n$,

$$Re[Z_R(k)] = R_R(k), \tag{35}$$

and

$$X_R(k) = Im[Z_R(k)]$$

is the radiation reactance given by the principal part (denoted by P) of the integral (34),

$$X_R(k) = P\{-\frac{1}{\pi} \int_0^\infty \frac{dk_n^2}{k^2 - k_n^2} R_R(k_n)\}. \tag{36}$$

Based on the above, the connection between the cavity impedance, represented by the sum in Eq. (32), and the radiation impedance, represented in Eq. (35) and Eq. (36), is as follows. The cavity impedance, Eq. (32), consists of a discrete sum over eigenvalues k_n with weighting coefficients w_n which are Gaussian random variables. There is an additional weighting factor $R_R(k_n)$ in the sum, which is the radiation resistance. The radiation reactance, Eq. (36), has a form analogous to the cavity impedance. It is the principle part of a continous integral over k_n with random coupling weights set to unity. While, Eqs. (32), (35), (36), have been obtained for the simple model imput $\hat{J} = \hat{I}u(x,y)$ in $0 \le z \le h$ with perfectly conducting plane surfaces at $z = 0, h$, we claim that these results apply in general. That is, for a case like that in Fig. 1(b), $Z_R(k)$ (which for the simple model is given by Eq. (34)) can be replaced by the radiation impedance for the problem with the same geometry. It is important to note that, while $R_R(k)$ is nonuniversal (i.e., depends on the specific coupling geometry, such as that in Fig. 2(b)), it is sometimes possible to independently calculate it, and it is also a quantity that can be directly measured (e.g., absorber can be placed adjacent to the lateral walls). In the next section, we will use the radiation impedance to normalize the cavity impedance yielding a universal distribution for the impedance of a chaotic cavity.

V. IMPEDANCE STATISTICS FOR A LOSSLESS, TIME REVERSAL SYMMETRIC CAVITY FED BY A SINGLE TRANSMISSION LINE

We first consider the time reversal symmetric (TRS) case for a lossless cavity with only one port. In this case, the impedance of the cavity Z in Eq. (32) is a purely imaginary number and S, the reflection coefficient, is a complex number with unit modulus. Terms in the summation of Eq. (32) for which k^2 is close to k_n^2 will give rise to large fluctuations in Z as either k^2 is varied or as one considers different realizations of the random numbers. The terms for which k^2 is far from k_n^2 will contribute to a mean value of Z. Accordingly, we write

$$Z = \bar{Z} + \tilde{Z}, \tag{37}$$

where $\bar{Z}$, the mean value of Z, is written as

$$\bar{Z} = -\frac{j}{\pi} \sum_n \Delta E\{\frac{R_R(k_n^2)}{k^2 - k_n^2}\}, \tag{38}$$

and we have used the fact that the w_n^2 are independent with $E\{w_n^2\} = 1$. If we approximate the summation in Eq. (38) by an integral, noting that Δ is the mean spacing between eigenvalues, comparison with (36) yields

$$\bar{Z} = jX_R(k), \tag{39}$$

where $X_R = Im[Z_R]$ is the radiation reactance defined by Eq. (36). Thus, the mean part of the fluctuating impedance of a closed cavity is equal to the radiation reactance that would be obtained under the same coupling conditions for an antenna radiating freely; i.e., in the absence of multiple reflections of waves from the lateral boundaries of the cavity.

As an example, we evaluate this impedance for the case of the annular current profile (30) in Appendix A and find

$$\bar{Z} = -j(kh\eta/4)J_0(ka)Y_0(ka), \tag{40}$$

where Y_0 is a Bessel function of the second kind. This impedance has a positive imaginary logarithmic divergence as $ka \to 0$ which is due to the large inductance associated with feeding the current through a small circle of radius a.

We now argue that, if k^2 is large enough that many terms in the sum defining Z satisfy $k_n^2 < k^2$, then the fluctuating part of the impedance $\tilde{Z}$ has a Lorentzian distribution with a characteristic width $R_R(k)$. That is, the probability density function for the imaginary part of the fluctuating

components of the cavity impedance $\tilde{Z} = j\tilde{X}$ is

$$P_{\tilde{X}}(\tilde{X}) = \frac{R_R}{\pi(\tilde{X}^2 + R_R^2)}. \tag{41}$$

The reason that the form of $P_{\tilde{X}}$ is Lorentzian will be given subsequently. That the characteristic width scales as $R_R(k)$ follows from the fact that the flucatuating part of the impedance is dominated by the terms for which $k_n^2 \simeq k^2$. The size of the contribution of a term in the sum in Eq. (32) decreases as $|k^2 - k_n^2|$ in the denominator increases. The many terms with large values of $|k^2 - k_n^2|$ contribute mainly to the mean part of the reactance with the fluctuations in these terms cancelling one and another due to the large number of such terms. The contributions to the mean part from the relatively fewer terms with small values of $|k^2 - k_n^2|$ tend to cancel due to the sign change of the denominator while their contribution to the fluctuating part of the reactance is significant since there are a smaller number of these terms. Consequently, when considering the impedance fluctuations, it suffices to treat $R_R(k_n)$ as a constant in the summation in Eq. (32) and factor it out. This results in a sum that is independent of coupling geometry and is therefore expected to have a universal distribution.

To test the arguments above, we consider a model normalized cavity reactance $\xi = X/R_R$ and also introduce a normalized wavenumber $\tilde{k}^2 = k^2/\Delta = k^2 A/4\pi$. In terms of this normalized wavenumber, the average of the eigenvalue spacing [average of $(\tilde{k}_{n+1}^2 - \tilde{k}_n^2)$] is unity. Our model normalized reactance is

$$\xi = -\frac{1}{\pi} \sum_{n=1}^{N} \frac{w_n^2}{\tilde{k}^2 - \tilde{k}_n^2}, \tag{42}$$

where the w_n are independent Gaussian random variables, $\tilde{k}_n^2$ are chosen according to various distributions, and we have set $R_R(k_n)$ to a constant value for $n \leq N$ and $R_R(k_n) = 0$ for $n > N$. The fluctuating part of $j\xi$ given by Eq. (42) mimics fluctuating part of the impedance Z in the case in which $R_R(k_n)$ as a sharp cut-off for eigenmodes with $n > N$. In terms of ξ, Eq. (41) becomes

$$P_\xi(\xi) = \frac{1}{\pi} \frac{1}{[(\xi - \bar{\xi})^2 + 1]}, \tag{43}$$

where $\bar{\xi}$ is the mean of ξ.

First we consider the hypothetical case where the collection of $\tilde{k}_n^2$ values used in Eq. (42) result from N independent and uniformly distributed random choices in the interval $0 \leqslant \tilde{k}_n^2 \leqslant N$. In contrast to Eqs. (3) and (4), this corresponds to a Poisson distribution of spacings $P(s) = exp(-s)$ for large N. In Appendix B, we show that this case is analytically solvable and that the mean

value $\bar{\xi}$ is

$$\bar{\xi} = P\{-\frac{1}{\pi} \int_0^N \frac{d\tilde{k}_n^2}{\tilde{k}^2 - \tilde{k}_n^2}\} = \frac{1}{\pi} ln |\frac{N - \tilde{k}^2}{\tilde{k}^2}|, \tag{44}$$

and, furthermore, that ξ has a Lorentzian distribution given by Eq. (43).

Our next step is to determine the probability distribution function for ξ given by (42) in the case where the spacing distribution corresponds to the TRS case described by Eq. (3). Since we have not been able to do this analytically, we do it numerically. Thus we generated 10^6 realizations of the sum in Eq. (42). For each realization we randomly generated $N = 2000$ eigenvalues using the spacing probability distribution (3), as well as $N = 2000$ random values of w_n chosen using a Gaussian distribution for w_n with $E\{w_n\} = 0$ and $E\{w_n^2\} = 1$. We first test the prediction of Eq. (44) by plotting the median value of ξ versus $\tilde{k}^2$ in Fig. 4(a). (We use the median rather than the mean, since, for a random variable with a Lorentzian distribution, this quantity is more robust when a finite sample size is considered.) Also plotted in Fig. 4(a) is the formula (44). We see that the agreement is very good. Next we test the prediction for the fluctuations in ξ by plotting a histogram of ξ values for the case $\tilde{k}^2 = N/2$ in Fig. 4(b). From (44) for $\tilde{k}^2 = N/2$ the mean is expected to be zero, and, as can be seen in the figure, the histogram (open circles) corresponds to a Lorentzian with zero mean and unit width (solid line) as expected. Histograms plotted for other values of $\tilde{k}^2$ agree with the prediction but are not shown. Thus, we find that the statistics of ξ are the same for $P(s) = exp(-s)$ (Poisson) and for $P(s)$ given by Eq. (3). Hence we conclude that the statistics of ξ are independent of the distribution of spacings. This is further supported by Fig. 4(c) where the histogram of ξ for $\tilde{k}^2 = N/2$ is plotted for the case in which the spacing distribution is that corresponding to time reversal symmetry broken (TRSB) systems, Eq. (4) (the TSRB case will be discussed more carefully in the next section). Again the histogram is in excellent agreement with (43). This implies that, for this case, with a single input transmission line to the cavity, the impedance statistics are the same for the TRS and TRSB cases. (This will not be so for cavities with more than one input port; see Sec. VI.)

Next we address the issue of long range correlations in the distribution of eigenvalues on statistics of the impedance. As we have mentioned, a quantity analogous to X, the "K-matrix", is considered in random matrix theory [35],

$$K = \pi W^\dagger (E - H)^{-1} W. \tag{45}$$

Here H is an N by N random matrix selected form the Gaussian Orthogonal Ensemble and W is an M by N random matrix whose elements are independent Gaussian random variables. K is thus an M by M square matrix. The parameter E is analogous to k^2 in our problem.
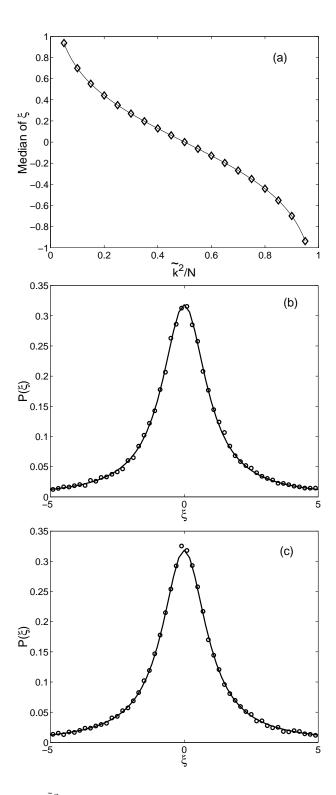
FIG. 4: (a) Median of ξ versus $\tilde{k}^2/N$, compared with Eq. (44). (b) Histogram of approximation to $P_\xi(\xi)$ (solid dots) in the TRS case compared with a Lorentzian distribution of unit width. (c) Same as (b) but for the TRSB case.

The similarity between K and Z defined in Eq. (26) is apparent if $(E - H)^{-1}$ is represented in the basis corresponding to the eigenvectors of H, $H = O\ diag(k_1^2,\ k_2^2,\ ... \ k_N^2)O^T$ where $O = [o_1|o_2|...|o_N]$, o_m is the mth eigenvector of H, $Ho_m = k_m^2 o_m$, $o_m^T o_{m'} = \delta_{mm'}$. The integers N and M play the role of the number of eigenmodes excited by the ports and the number of ports respectively. For example, in the one port case, W is an N-dimensional column vector, and Eq. (45) becomes

$$K = \pi \sum_{n=1}^{N} \frac{\tilde{w}_n^2}{k^2 - k_n^2}, \tag{46}$$

where $\tilde{w}_n = W^T o_n$, and we have replaced E by k^2. The formal equivalence between ξ in (42) and K is apparent ($-\pi\xi \Leftrightarrow K/\pi$, $w_n^2 \Leftrightarrow \tilde{w}_n^2$). Thus, the random plane wave hypothesis corresponds to $W^T o_n$ being a Gaussian random number. One of the most important differences between our formulation and random matrix theory is that in some cases we ignore the long range correlations among eigenvalues, i.e., the spacings are taken to be independent of each other, whereas the eigenvalues of the random matrix H (and resonant cavities) have long range correlations. Nevertheless Ref. [35] shows that the eigenvalues of K are Lorentzian distributed. (For the case $M=1$ corresponding to a single port, the value K is Lorentzian distributed.) Therefore the appearance of a Lorentzian is not dependent on long range correlations of the k_n^2 (analogously the eigenvalues of H). We emphasize that our use of only the nearest neighbor statistics to model the statistical properties of k_n^2 is mostly motivated by the resulting ease of numerical implementation and our conjecture that it will yield accurate results for the impedance statistics. As will subsequently become apparent, this is very well supported by our numerical experiments. However, we note that in principle, one can also incorporate additional eigenvalue correlation from random matrix theory in the statistics generating the k_n^2 in Eq. (42).(and when losses are considered, this is necessary.) We note that the mean and width of the distribution in the random matrix approach are specific to the random matrix problem. In contrast, in our formulation, these quantities are determined by the geometry specific port coupling to the cavity through the radiation impedance $Z_R(k_n^2)$.

To test our prediction for the distribution function of the normalized impedance we have computed the impedance for the cavity in Fig. 3(a) for the coupling shown in Fig. 3(b) using the commercially available program HFSS (High Frequency Structure Simulator). To create different realizations of the configuration, we placed a small metallic cylinder of radius 0.6 cm and height h at 100 different points inside the cavity. In addition, for each location of the cylinder, we swept the frequency through a 2.0 GHz range (about 100 modes) from 6.75GHz to 8.75GHz in 4000 steps of width 5×10^{-4} GHz. We generated 100,000 impedance values. In addition, to obtain the radiation
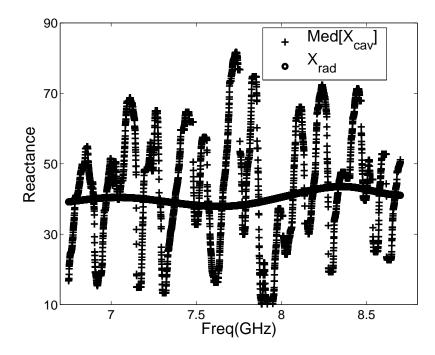
FIG. 5: Median cavity reactance averaged over 100 realization vs. frequencies ranged from 6.75GHz to 8.75GHz, compared with the corresponding radiation reactance $Im[Z_R(\omega)]$.

impedance, we also used HFSS to simulate the case with absorbing boundary conditions assigned to the sidewalls of the cavity. We find that the average value of the cavity reactance (which we predict to be the radiation reactance) has large systematic fluctuations. This is illustrated in Fig. 5 where we plot the median cavity reactance versus frequency. Here the median is taken with respect to the 100 locations of the perturbing disc. Also shown in Fig. 5 is the radiation reactance $X_R(\omega) = Im[Z_R(\omega)]$. As can be seen the radiation reactance varies only slightly over the plotted frequency range, whereas the median cavity reactance has large frequency dependent fluctuations about this value. On the other hand, we note that over the range 6.75-8.75 GHz, the average radiation reactance is 40.4 Ω and the average of the median cavity reactances is 42.3Ω. Thus over this frequency band, there is good agreement. The scale of the fluctuations in cavity reactance is on the order of 0.2GHz, which is much larger than the average spacing between cavity resources which is only 0.016GHz. Thus, these fluctuations are not associated with individual resonances. Rather, the frequency scale of 0.2GHz suggests that they are multipath interference effects ($L \sim 100cm$), which survive in the presence of the moveable conducting disc. One possibility is that the fluctuations are the result of scars and this will be investigated in the future. The implication is that to obtain good agreement with the theory predicting Lorentzian distribution, it may be necessary to average over a sufficiently large frequency interval.
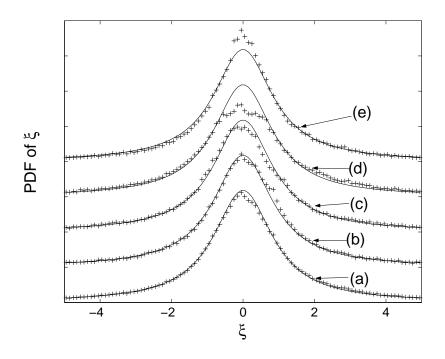
FIG. 6: Histogram approximation to $P_\xi(\xi)$ from numerical data calculated using HFSS in different frequency ranges. (a) 6.75 - 8.75 GHz, (b) 6.75 - 7.25 GHz, (c) 7.25 - 7.75GHz, (d) 7.75 - 8.25 GHz, (e) 8.25 - 8.75 GHz.

To test the Lorentzian prediction we normalize the cavity impedance using the radiation impedance as in Eq. (39) and Eq. (41), the normalized impedance values, $\tilde{\xi} = \{\text{Im}[Z(k)] - X_R(k)]\}/R_R(k)$, are computed, and the resulting histogram approximations to $P_\xi(\tilde{\xi})$ is obtained. Fig. 6(a) shows the result for the case where we have used data in the frequency range 6.75GHz to 8.75GHz (the range plotted in Fig. 5). The histogram points are shown as dots, and the theorectical unit width Lorentzian is shown as a solid curve. Good agreement between the predicted Lorentzian and the data is seen. Figures 6 (b)-(e) show similar plots obtained for smaller frequency range of width 0.5GHz: (b) 6.75 - 7.25 GHz, (c) 7.25 - 7.75GHz, (d) 7.75 - 8.25 GHz, (e) 8.25 - 8.75 GHz. For these narrow freqency ranges, we see that Figs. 6(b) and 6(c) show good agreement with (43), while, on the other hand, Figs. 6(d) and 6(e) exhibit some differences.

We now summarize the main ideas of this section. The normalized impedance of a chaotic cavity with time-reversal symmetry has a universal distribution which is a Lorentzian. The width of the Lorentzian and the mean value of the impedance can be obtained by measuring the corresponding radiation impedance under the same coupling conditions. The physical interpretation of this correspondence is as follows. In the radiation impedance, the imaginary part is determined by the near field, which is independent of cavity boundaries. On the other hand, the real part

of the radiation impedance is related to the far field. In a closed, lossless cavity, the real part of the impedance vanishes. However, waves that are radiated into the cavity are reflected from the boundaries eventually returning to the port and giving rise to fluctuation in the cavity reactance.

VI.   GENERALIZATION: THE STATISTICS OF Z MATRICES

In the previous two sections, we restricted our considerations to discussion of the simplest case, that of a one-port, time-reversal symmetric, lossless cavity. In this section, we will generalize our model to describe the impedance matrix in more complicated situations. The implications of our theory for scattering matrices are discussed in Sec. VII.

A.   Lossless multiport case with time reversal symmetry

In the one port case, there is only one driving source $u\hat{I}$ in Eq. (23). For the multiport case, we suppose $u_i(x, y)$ is the profile function for i-th port and each port is driven independently by a current $\hat{I}_i$. Then Eq. (23) becomes

$$(\nabla_\perp^2 + k^2)\hat{V}_T = -jkh\eta_0 \sum_{i=1}^{M} u_i\hat{I}_i, \tag{47}$$

where $\int dxdy u_i = 1$ and M is the number of ports. Each of the u_i are centered at different locations. The phasor voltage at each port can be calculated as before, $\hat{V}_i = \int dxdy u_i\hat{V}_T \equiv <u_i\hat{V}_T>$ and is linearly related to the phasor currents $\hat{I}_j$ through the impedance matrix, $\hat{V}_i = \sum_j Z_{ij}\hat{I}_j$.

To obtain an expression for the matrix Z, we expand $\hat{V}_T$ as before in the basis ϕ_n, the result is

$$Z = -jkh\eta_0 \sum_n \frac{\Phi_n\Phi_n^T}{k^2 - k_n^2}, \tag{48}$$

where the vector Φ_n is $[\langle u_1\phi_n\rangle, \langle u_2\phi_n\rangle, ..., \langle u_M\phi_n\rangle]^T$. Using the random eigenfunction hypothesis, we write Φ_n as

$$\Phi_n = L(k_n)w_n, \tag{49}$$

where L is a nonrandom, as yet unspecified, $M \times M$ matrix that depends on the specific coupling geometry at the ports and may depend smoothly on k_n, and w_n is an M-dimensional Gaussian random vector with covariance matrix $C(k_n)$. That is, the probability distribution of w_n is

$$P_w(w_n) \propto exp - (\frac{1}{2}w_n^T C(k_n)^{-1}w_n). \tag{50}$$

27

Note that $C(k_n) = \int P_w(w_n) w_n w_n^T dw_n \equiv \langle w_n w_n^T \rangle$. We desire to choose $L(k)$ so that $C(k) = 1_M$, where 1_M is the $M \times M$ identity matrix. That is, we require that the components of the random vector are statistically independent of each other, each with unit variance. The idea behind (49) is that the excitation of the ports by an eigenmode will depend on the port geometry and on the structure of the eigenmode in the vicinity of the ports. The dependence on the specific port geometry is not sensitive to small changes in the frequency or cavity configuration and is embodied in the matrix quantity $L(k)$. The structure of the eigenmode in the vicinity of the ports, however, is very sensitive to the frequency and cavity configuration, and this motivates the statistical treatment via the random plane wave hypothesis. From the random plane wave hypothesis, the excitation of the port from a given plane wave component is random, and, since many such waves are superposed, by the central limit theorem, the port excitation is a Gaussian random variable, as reflected by the vector w_n. In Sec. IV we have derived a result equivalent to (49) for the case of a one-port with a specific model of the excitation at the port (namely, a vertical source current density $Iu(x,y)\hat{z}$ between the plates). Our derivation here will be more general in that it does not depend on a specific excitation or on the two-dimensional cavity configuration used in Sec. IV. Thus this derivation applies, for example, to three dimensional cavities, and arbitrary port geometries. From (48) and (49) we have

$$Z = -jkh\eta_0 \sum_n \frac{L(k_n) w_n w_n^T L^T(k_n)}{k^2 - k_n^2}. \tag{51}$$

We now take the continuum limit of (51) and average over w_n,

$$\langle Z \rangle = -j \int_0^\infty kh\eta_0 L(k') \frac{C(k')}{k^2 - (k')^2} L^T(k') \frac{dk'^2}{\Delta}. \tag{52}$$

We note that the continuum limit is approached as the size of the cavity is made larger and larger, thus making the spacing $(k_{n+1}^2 - k_n^2)$ approach zero. Thus, the continuum limit corresponds to moving the lateral walls of the cavity to infinity. Using our previous one-port argument as a guide, we anticipate that, if the pole in Eq. (52) at $k'^2 = k^2$ is interpreted in the causal sense (corresponding to outgoing waves in the case with the walls removed to infinity), then $\langle Z \rangle$ in (52) is the radiation impedance matrix,

$$\langle Z \rangle = Z_R(k) = R_R(k) + jX_R(k), \tag{53}$$

where $\hat{V} = Z_R(k)\hat{I}$ with $\hat{V}$ the M-dimensional vector of port voltages corresponding to the M-dimensional vector of port currents $\hat{I}$, in the case where the lateral walls have been removed to infinity. With the above interpretation of the pole, the real part of Eq. (52) yields

$$R_R(k) = \pi kh\eta_0 L(k) C(k) L^T(k)/\Delta. \tag{54}$$

28

Choosing $L(k)$ to be

$$L(k) = [\frac{\Delta}{\pi k h \eta_0} R_R(k)]^{\frac{1}{2}}, \tag{55}$$

where the positive symmetric matrix square root is taken, Eq. (54) yields $C(k) = 1_M$, as desired. Thus, Eq. (48) becomes

$$Z = -\frac{j}{\pi} \sum_n \Delta \frac{R_R^{1/2}(k_n) w_n w_n^T R_R^{1/2}(k_n)}{k^2 - k_n^2}, \tag{56}$$

where $< w_n w_n^T >= 1_M$. (Note that the Weyl formula for Δ is different in two and three dimensions.) In the case of transmission line inputs that are far apart, e.g., of the order of the cavity size, then the off-diagonal elements of Z_R are small and can be neglected. On the other hand, this will not be the case if some of the transmission line inputs are separated from each other by a short distance of the order of a wavelength. Similarly, if there is a waveguide input to the cavity where the waveguide has multiple propagating modes, then there will be components of $\hat{V}$ and $\hat{I}$ for each of these modes, and the corresponding off-diagonal elements of Z_R for coupling between these modes will not be small.

For the remainder of the paper, we will assume identical transmission line inputs that are far enough apart that we may neglect the off-diagonal elements of Z_R. As before, we will take the eigenvalues k_n^2 to have a distribution generated by the spacing statistics. Because the elements of Z depend on the eigenvalues k_n^2, there will be correlations among the elements. The elements of the Z matrix are imaginary, $Z = jX$, where X is a real symmetric matrix. Consequently X has real eigenvalues. We will show in Sec. IV.C that the distribution for individual eigenvalues of X is Lorentzian with mean and width determined by the corresponding radiation impedance.

B. Effects of Time-Reversal Symmetry Breaking (TRSB)

In the time-reversal symmetric system, the eigenfunctions of the cavity are real and correspond to superpositions of plane waves with equal amplitude waves propagating in opposite directions as in Eq. (27). If a non-reciprocal element (such as a magnetized ferrite) is added to the cavity, then time reversal symmetry is broken (TRSB). As a consequence, the eigenfunctions become complex. Eq. (27) is modified by removal of the operation of taking the real part, and the $\langle u_i \phi_n \rangle$ in Eq. (26) also become complex. In this case we find

$$\langle u_\ell \phi_n \rangle = [\Delta R_R(k_n)]^{1/2} w_{\ell n} \tag{57}$$

29

where $w_{\ell n} = (w_{\ell n}^{(r)} + j w_{\ell n}^{(i)})/\sqrt{2}$ and $w_{\ell n}^{(r)}$ and $w_{\ell n}^{(i)}$ are real, independent Gaussian random variables with zero mean and unit variance. The extra factor of $\sqrt{2}$ accounts for the change in the normalization factor in Eq. (27), required when the eigenfunctions become complex. Further, w_n^T in Eq. (56) and Eq. (50) is now replaced by $w_n^\dagger$.

A further consequence of TRSB is that the distribution of eigenvalue spacings is now given by Eq. (4), rather than by (3). The main difference between Eq. (3) and Eq. (4) is the behavior of $P(s)$ for small s. In particular, the probability of small spacings in a TRSB system (4) is less than than of a TRS system (3) ($P(s) \sim s^2$ rather than s).

For the sake of simplicity, we will assume all the transmission lines feeding the cavity ports are identical, and have the same radiation impedance ($R_R + jX_R$). Analogous to the one port case, we can define a model normalized reactance matrix $\xi_{ij} = X_{ij}/R_R$ for the case $R_R(k_n)$ constant for $n \leq N$ and $R_R(k_n) = 0$ for $n > N$,

$$\xi_{ij} = -\frac{1}{\pi} \sum_{n=1}^{N} \frac{w_{in} w_{jn}^*}{\tilde{k}^2 - \tilde{k}_n^2}, \tag{58}$$

where $\tilde{k}^2 = k^2/\Delta$, $w_{\ell n} = (w_{\ell n}^{(r)} + j w_{\ell n}^{(i)})/\sqrt{2}$, $w_{\ell n}^{(r)}$ and $w_{\ell n}^{(i)}$ are real, independent Gaussian random variables with zero mean and unit variance, $E(w_{in}^* w_{jn}) = \delta_{ij}$. Note that a unitary transformation, $\xi' = U\xi U^\dagger$, returns (58) with w_{in} and w_{jn} replaced by w_{in}' and w_{jn}' where $w_n' = U w_n$. Since a unitary transformation does not change the covariance matrix, $E(w_{in} w_{jn}^*) = E(w_{in}' w_{jn}'^*) = \delta_{ij}$, the statistics of ξ and of ξ' are the same; i.e., their statistical properties are invariant to unitary transformations.

C. Properties of the impedance matrix

The fluctuation properties of the Z matrix can be described by the model matrix ξ_{ij} specified in Eq. (58). In the TRS case the w_{jn} are real Gaussian random variables with zero mean and unit width and the spacings of the k_n^2 satisfy (3). In the TRSB case the w_{jn} are complex and the spacings between adjacent k_n^2 satisfy (4).

In the case under consideration of multiple identical ports, ξ_{ij} will have a diagonal mean part $\bar{\xi} \delta_{ij}$ for which all the diagonal values are equal and given by (44). The eigenfunctions of $\xi_{ij} = \bar{\xi} \delta_{ij} + \tilde{\xi}_{ij}$ and of its fluctuating part $\tilde{\xi}_{ij}$ will thus be the same. Consequently, we focus on the eigenvalues of the fluctuating part.

We restrict our considerations to the two-port case. We recall that for the one-port case there is no difference in the statistics of Z for the TRS and TRSB cases. In the two-port case, how-
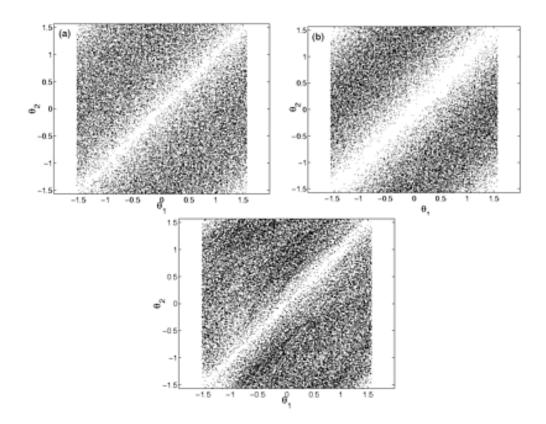
FIG. 7: (a) Scatter plot of θ_1 vs θ_2, in the TRS case. (b) Scatter plot of θ_1 vs θ_2 in the TRSB case.(c) Scatter plot of θ_1 vs θ_2 from the HFSS simulation, with 100 realizations and sweeping freqency from 6.75GHz to 8.75GHz.

ever, essential differences are observed when time reversal is broken. Using (58) we generate 10^6 realizations of the 2 by 2 matrix ξ in both the TRS and TRSB cases, again for $N = 2000$ and $k^2 = 1000$. For each realization we compute the eigenvalues of the ξ matrix. Individually the probability distributions of the eigenvalues are Lorentzian. However, if we consider the joint probability density function (PDF) of the two eigenvalues, then differences between the TRS and TRSB cases emerge. We map the two eigenvalues ξ_i, $i = 1$ or 2, into the range $[\pi/2, \pi/2]$ via the transformation $\theta_i = \arctan(\xi_i)$. Scatter plots of θ_2 and θ_1 for 10^6 realizations of the ξ matrix are shown in Fig. 7(a) for the TRS case and in Fig. 7(b) for the TRSB case. The white diagonal band in both cases shows that the eigenvalues avoid each other (i.e., they are anti-correlated). This avoidance is greater in the TRSB case than in the TRS case. The correlation

$$corr(\theta_1, \theta_2) \equiv \frac{\langle \theta_1 \theta_2 \rangle - \langle \theta_1 \rangle \langle \theta_2 \rangle}{\sqrt{\langle \theta_1^2 \rangle \langle \theta_2^2 \rangle}} \tag{59}$$

is -0.216 for the TRS case and -0.304 for the TRSB case.

From the construction of the ξ matrices for the TRS and TRSB cases their statistical properties

31

are invariant under orthogonal and unitary transformations, respectively. Random matrix theory has been used to study these rotation-invariant ensembles and predicts the joint density function of θ_1 and θ_2 [35] to be,

$$P_\beta(\theta_1, \theta_2) \propto |e^{j2\theta_1} - e^{j2\theta_2}|^\beta, \tag{60}$$

where $\beta = 1$ for the TRS case and $\beta = 2$ for the TRSB case. Note that based on Eq. (60), the probability density function for one of the angles $P(\theta_1) = \int d\theta_2 P(\theta_1, \theta_2)$ is uniform. From the definition $\theta = \arctan\xi$, this is equivalent to the eigenvalues of the ξ matrix having Lorentzian distributions $(P_\xi(\xi_i) = P_\theta(\theta_i)|d\theta_i/d\xi_i| = |d\theta_i/d\xi_i|/2\pi)$.

The correlation coefficients calculated from the numerical results in Figs. 7(a) and 7(b) are consistent with the predictions of the random matrix theory from Eq. (60), that is, -0.216 for the TRS case and -0.304 for the TRSB case. This implies that the distribution of spacings and the long range correlations in the eigenvalues of the random matrix, which are ignored in the construction of the k_n^2 in our Random Coupling Model, are not important in describing the statistics of the impedance matrix. (These correlations can be included using a sequence of k_n^2 generated by the eigenvalues of a random matrix.)

Now we test these predictions for our Bow-tie cavity of Fig. 3. We use the HFSS software to calculate the cavity impedance matrix and radiation impedance matrix for a 2-port case. We locate the two ports, of the kind pictured in Fig.3(b), at the positions (x, y)=(14cm, 7cm) and (x, y)=(27cm, 13.5cm). We also include the 0.6cm cylindrical perturbation which is located alternately at 100 random points in the cavity, and we numerically calculate the impedance matrix for 4000 frequencies in the range 6.75GHz to 8.75GHz. We obtain a normalized Z matrix, which is analogous to the ξ matrix defined in Eq. (58) according to

$$\xi_{hfss} = R_R^{-1}(Im[Z_{cav}] - \tilde{1}X_R), \tag{61}$$

where $\tilde{1}$ is the 2 by 2 identity matrix, Z_{cav} is the 2 by 2 impedance matrix calculated by HFSS, and X_R and R_R are the radiation reactance and resistance for a single port. For each realization of ξ_{hfss} we calculate its eigenvalues $\xi_i = \tan\theta_i$, $i = 1, 2$, and plot the values on the θ_1 vs. θ_2 plane, as shown in Fig. 7(c). The anti-correlation of the angles is seen in the figure, and $corr(\theta_1, \theta_2)$ from (59) is -0.205, which is comparable with what we expect for the TRS case, -0.216.

So far we have focused on the eigenvalues of the impedance matrix. The eigenfunctions of Z are best described in terms of the orthogonal matrix whose columns are the orthonormal eigenfunctions

of Z. Specially, in the TRS case, since ξ is real and symmetric,

$$\xi = O \begin{pmatrix} \tan\theta_1 & 0 \\ 0 & \tan\theta_2 \end{pmatrix} O^T, \tag{62}$$

where O^T is the transpose of O, and O is an orthogonal matrix, which we express in the form

$$O = \begin{pmatrix} \cos\eta & \sin\eta \\ -\sin\eta & \cos\eta \end{pmatrix}. \tag{63}$$

A scatter plot representing the joint pdf of the angle η and one of the eigenvalue angles θ_1 is shown in Fig. 8(a1). In analogy to how we obtain the realizations used in Fig. 4, this plot is obtained by inserting random choices for the k_n^2 and w_{in} in (58). Notice that we have restricted η in Fig. 8(a1) to the range $0 \le \eta \le \pi/2$. This can be justified as follows. The columns of the matrix O in (63) are the eigenvectors of ξ. We can always define an eigenvector such that the diagonal components of O are real and positive. Further, since the eigenvectors are orthogonal, one of them will have a negative ratio for its two components. We pick this one to be the first column and hence this defines which of the two eigenvalues is θ_1. The scatter plots in Fig. 7 show that the restriction on η maintains the symmetry of θ_1 and θ_2, vis. $P_\beta(\theta_1, \theta_2) = P_\beta(\theta_2, \theta_1)$. Also in the Fig. 8(a2) (and (a3)), we plot the conditional distribution of θ (and η) for different values of η (and θ). As can be seen, these plots are consistent with η and θ being independent. This is also a feature of the random matrix model [18]. This independence will be exploited later when the S matrix is considered.

For TRSB systems, the ξ matrix is Hermitian $\xi^T = \xi^*$. A unitary matrix of eigenvectors that diagonalizes it can be parameterized as

$$U = \begin{pmatrix} \cos\eta & \sin\eta\, e^{i\zeta} \\ -\sin\eta\, e^{-i\zeta} & \cos\eta \end{pmatrix}. \tag{64}$$

Thus, there is an extra parameter ζ characterizing the complex eigenvectors of the ξ matrix. According to random matrix theory, the eigenfunctions and eigenvalues are independently distributed, i.e. η in the U matrix should be independent of θ_1, θ_2. This expectation is confirmed in Fig. 8(b) where a scatter plot of θ_1 vs η and conditional distributions of θ and of η are shown.

Again, we test the independence of θ and η with HFSS calculations. Using the ξ_{hfss} matrix obtained from Eq. (61), the angles θ and η can be recovered from the eigenvalues and the eigenvectors of the ξ_{hfss}. With the ensemble generated by sweeping the frequency from 6.75-8.75GHz and considering 100 different locations of our cylindrical perturber, we obtain the joint distribution of θ
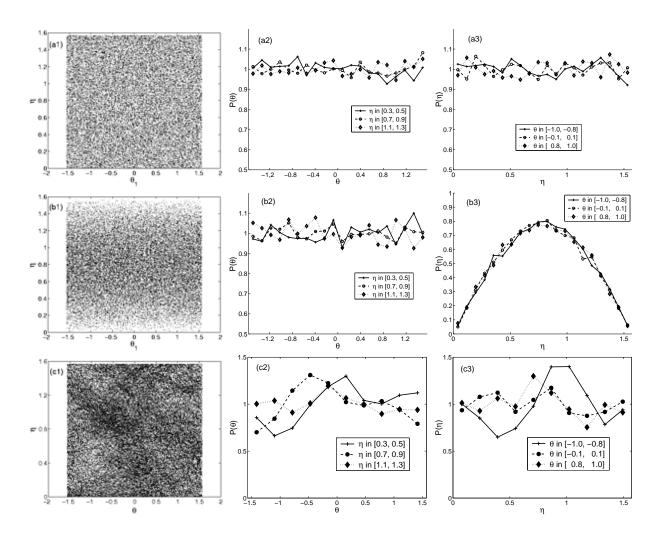
33

FIG. 8: Scatter plot of η vs θ for (a1) the model impedance in the TRS case, (b1) the model impedance in the TRSB case, and (c1) from the HFSS simulation. Plots (a2) and (a3) [(b2) and (b3), (c2) and (c3)] show conditional probability for θ and for η for the model TRS case [model TRSB case, the HFSS simulation].

and η in Fig. 8(c1) as well as their individual distributions in Fig. 8(c2) and (c3). Here we see that the distributions are qualitatively similar to those of the model impedance matrix in the TRS case. However, there are significant departures which need to be investigated. It is likely that these are the result of the same strong multipath interference which gave rise to the reactance variations in Fig. 5.

D. Variations in Coupling

We have argued that the result, Eq. (32), is general (see also Sec. VI.A). We now further address this issue by considering the external coupling to the cavity. Let us suppose a one-port coupling case in which the actual coupling is equivalent to the cascade of a lossless two port and
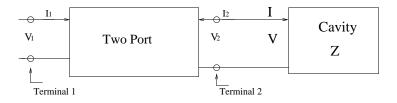
FIG. 9: Schematic description of the two port model

a "pre-impedance" Z seen at the terminal 2, as illustrated in Fig. 9.

The impedance Z of the cavity at terminal 2 then transforms to a new impedance Z' at terminal 1 of the two port according to

$$Z' = j\hat{X}_{11} + \frac{\hat{X}_{12}\hat{X}_{21}}{j\hat{X}_{22} + Z}, \tag{65}$$

where $j\hat{X}_{ij}$ is now the purely imaginary 2 by 2 impedance matrix of the lossless two-port. We now ask how Z transforms to Z' when (a) Z is the complex impedance Z_R corresponding to the radiation impedance into the cavity (i.e. the cavity boundaries are extended to infinity) and (b) $Z = jX$ is an imaginary impedance corresponding to a lossless cavity, where X has a mean $\bar{X}$ and Lorentzian distributed fluctuation $\tilde{X}$.

First considering case (a) the complex cavity impedance $Z_R = R_R + jX_R$ transforms to a complex impedance $Z'_R = R'_R + jX'_R$ where

$$R'_R = R_R \frac{\hat{X}_{12}\hat{X}_{21}}{R_R^2 + (\hat{X}_{22} + X_R)^2}, \tag{66}$$

and

$$X'_R = \hat{X}_{11} - (\hat{X}_{22} + X_R)\frac{\hat{X}_{12}\hat{X}_{21}}{R_R^2 + (\hat{X}_{22} + X_R)^2}. \tag{67}$$

In case (b) we consider the transformation of the random variable X to a new random variable X' according to $X' = \hat{X}_{11} + \hat{X}_{12}\hat{X}_{21}/(\hat{X}_{22} + X)$. One can show that if X is Lorentzian distributed with mean X_R and width R_R then X' will be Lorentzian distributed with mean X'_R and the width R'_R. Thus, the relation between the radiation impedance and the fluctuating cavity impedance is preserved by the lossless two port. Accordingly, we reassert that this relation holds in general for coupling structures whose properties are not affected by the distant walls of the cavity.

E. Effect of distributed losses

We now consider the effect of distributed losses in the cavity. By distributed losses, we mean losses that affect all modes in a frequency band equally (or at least approximately so). For example,

wall losses and losses from a lossy dielectric that fills the cavity are considered distributed. [For the case of losses due to conducting walls, the losses are approximately proportional to the surface resistivity, $\sim \sqrt{f}$, and vary little in a frequency range $\Delta f \ll f$. In addition, there will also be variation of wall losses from mode to mode due to different eigenmode structural details. These modal fluctuations, however, are small when the modes are chaotic and the wavelength is short.] We use the random coupling model to construct a complex cavity impedance matrix accounting for distributed analogous to lossless case, Eq. (56),

$$\mathbb{Z} = -\frac{j}{\pi} \sum_n \Delta \frac{R_R^{1/2}(k_n) w_n w_n^T R_R^{1/2}(k_n)}{k^2(1 - j\sigma) - k_n^2},$$
(68)

where σ represents the effect of losses. In particular, for loss due to wall absorption in a two-dimensional cavity, the value of σ is equal to the ratio of the skin depth of the conductor to the height of the cavity; if the cavity contains a lossy dielectric, σ is the loss tangent of the dielectric. The cavity quality factor is related to σ by $\sigma = Q^{-1}$. This follows by noting the real part of Z will have a Lorenzian depedence on frequency ($\omega = kc$) peaking at $w = k_n c$ with a full width at half maximum of $\omega\sigma$.

We first investigate a model, normalized impedance, applicable in the one-port case, which is the generalization of Eq. (42),

$$\zeta(\sigma) = -\frac{j}{\pi} \sum_{n=1}^{N} \frac{w_n^2}{\tilde{k}^2(1 - j\sigma) - \tilde{k}_n^2}.$$
(69)

The normalized impedance ζ will have a real part $\rho > 0$ and an imaginary part ξ, $\zeta = \rho + j\xi$. We expect that if $\tilde{k}^2\sigma \ll 1$, corresponding to small loss, $\rho \cong 0$, and ξ will have an approximately Lorentzian distribution.

As losses are increased such that $\tilde{k}^2\sigma \sim 1$ [the imaginary part of the denominator in Eq. (69) is comparable to the spacing in eigenvalues $\tilde{k}_n^2$ (whose average spacing is one)], the distributions of both ξ and ρ will change, reflecting the fact that the extremely large values of $|\zeta|$ are no longer likely. For $1 \ll \tilde{k}^2\sigma \ll N$ many terms in the sum will contribute to the value of ζ. In this case, we expect $\zeta(\sigma)$ will approach the radiation impedance with relatively small (Gaussian) fluctuations. We will find that with losses present the only long range corrllations in the eigenvalues expected on the basis of random matrix theory have a quantitative effect on the distributions of ρ and ξ. This can be calculated analytically in the high loss case $1 \ll k^2\sigma \ll N$ and is included in Appendix C. To gain insight, however, we will first consider spectra generated by sequences of uncorrellated separations.
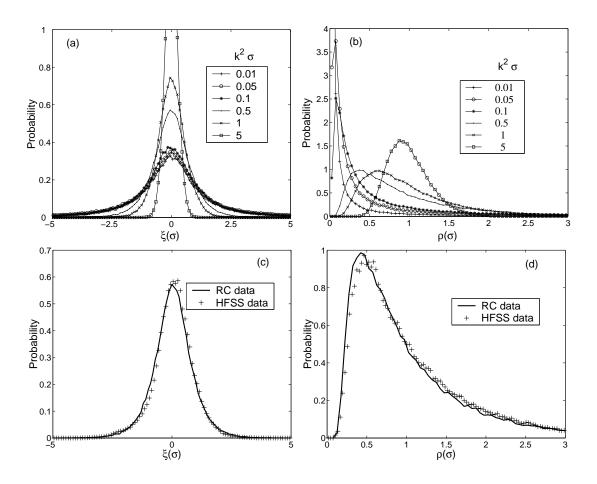
FIG. 10: (a) Histogram of the imaginary part of $\zeta(\sigma)$ with different values of the damping; (b) Histogram of the real part of $\zeta(\sigma)$ with different dampings, where $\tilde{k}^2 = 1000$ in the simulations.(c) and (d) are Histograms of the reactance and resistance from HFSS calculation with a lossy top and bottom plate, compared with the histogram from Random Coupling Model with parameter $\tilde{k}^2\sigma = 0.5$.

Histograms of the real and imaginary parts of ζ are shown in Fig. 10 for the case of 10^6 realizations of (69) with $N = 2000$ and different values of $\tilde{k}^2\sigma$. As mentioned spectra k_n^2 are generated assuming independent spacings. Here we choose the special value $\tilde{k}^2 = N/2 = 1000$ such that the corresponding radiation impedance has zero reactance. The general trends described above are born out. Figures 10(a) and 10(b) show histograms constructed by joining straight line segments between adjacent points. As seen in Fig. 10(a), when $\tilde{k}^2\sigma$ is increased, the distribution of ξ values becomes "squeezed". Namely, the Lorentzian tail disappears and the fluctuations in ξ decrease. Eventually, when σ enters the regime, $1 \ll \tilde{k}^2\sigma \ll N$, the probability distribution function of $\xi(\sigma)$ approaches a narrow normal distribution centered at $\xi = 0$ (recall that $\bar{\xi} = 0$). As shown in Fig. 10(b), as σ increases from zero, the distribution of the real part of $\zeta(\sigma)$ which, for $\sigma = 0$, is a delta function at zero, expands and shifts toward 1, becoming peaked around 1.

Using HFSS, we simulate the lossy case by specifying the material on the top and bottom plates to be an imperfect conductor with a bulk resitivity of 70 $m\Omega \cdot cm$. In this case we can calculate a value of $\sigma = \delta/h = 0.002$, where δ is the skin depth and h the cavity height. The corresponding parameter $\tilde{k}^2\sigma$ is 0.5 at 7.75GHz. Histogram results for the normalized reactance (ξ) and resistance (ρ) fluctuations of $\zeta_{hfss} = R_R^{-1}(Z_{cav} - jX_R) = \rho + j\xi$ are plotted in Figs. 10(c) and 10(d) together with the histograms from the random coupling model, Eq. (69), with $\tilde{k}^2\sigma = 0.5$. As can be seen the histograms from the HFSS simulations match those of the random coupling model.

We now focus on the effect of different eigenvalue distributions by considering the case of high damping($N \gg k^2\sigma \gg 1$). In the high damping case, the fluctuating part of ξ give by (69)is determined by contributions from the sum of a relatively large number of terms satisfying $|\tilde{k}^2 - \tilde{k}_n^2| \sim k^2\sigma \gg 1$. Given the independence of the w_n we therefore expect ξ to be a Gaussian random variable, and it is thus sufficient to calculate its mean and variance. The calculation is carried out in Appdendix C. We find in the range $\Delta \sim k^2\sigma \ll k^2$, that the expected value of the cavity impedance is the radiation impedance,

$$E[Z] = R_R(k^2) + jX_R(k^2). \tag{70}$$

The variance of the real and imaginary parts of the cavity impedance are given in Appendix C in terms of the two-eigenvalue correlation functions. When the damping is large, $\Delta \ll k^2\sigma \ll k^2$, the variance of R and X are given by

$$Var[R] = Var[X] = R_R^2 \frac{C\Delta}{k^2\sigma}, \tag{71}$$

where $C = 3/2\pi$ for the case of Poisson distributed independent spacings, $C = 0.7577 \times 3/2\pi$ for the case of independent spacings with TRS spacing distributions, and $C = 1/\pi$ for the case of spectra corresponding to random matrices.

VII. S MATRIX STATISTICAL PROPERTIES

In this section, we use our knowledge of the statistical properties of the Z matrix to infer properties of the S matrix. In particular, we will consider the distribution of values of the magnitude and phase of the S matrix elements.

A. One Port Case

For the one port lossless case the S matrix is a complex number with unit modulus. What is relevant then is the phase of S, which can be related to the imaginary cavity impedance and the characteristic impedance Z_0 of the transmission line feeding the cavity. We assume that the signal is in a narrow range of frequencies such that $Z_R = R_R + jX_R$ is essentially constant. We then use our model (37), (39) and (41) to express the cavity impedance Z,

$$Z = j(X_R + \tilde{\xi}R_R), \tag{72}$$

where $\tilde{\xi}$ is a unit width, zero mean, Lorentzian distributed random variable. From (72),

$$S = e^{j\phi} = (Z + Z_0)^{-1}(Z - Z_0) = \frac{j(\gamma_R\tilde{\xi} + \gamma_X) - 1}{j(\gamma_R\tilde{\xi} + \gamma_X) + 1}, \tag{73}$$

where

$$\gamma_R = R_R/Z_0, \quad \gamma_X = X_R/Z_0.$$

We replace the Lorentzian random variable $\tilde{\xi}$ by introducing another random variable ψ via $\tilde{\xi} = \tan(\psi/2)$. Using this substitution, the Lorentzian distribution of $\tilde{\xi}$ translates to a distribution of ψ that is uniform in $[0, 2\pi]$. We then have from Eq. (73)

$$e^{j(\phi-\phi_R)} = \frac{e^{-j\psi'} + |\rho_R|}{1 + |\rho_R|e^{-j\psi'}}, \tag{74}$$

where the "free space reflection coefficient" ρ_R

$$\rho_R = |\rho_R|e^{j\phi_R} = \frac{\gamma_R + j\gamma_X - 1}{\gamma_R + j\gamma_X + 1}, \tag{75}$$

is the complex reflection coefficient in the case in which the cavity impedance is set equal to the radiation impedance ($\tilde{\xi} = -j$), and $\psi' = \psi + \pi + \phi_R + 2\tan^{-1}[\gamma_X/(\gamma_R + 1)]$ is a shifted version of ψ. Equations for the magnitude and phase of the free space reflection coefficient ρ_R can be obtained from Eq. (75). Specifically,

$$|\rho_R| = \sqrt{\frac{(\gamma_R - 1)^2 + \gamma_X^2}{(\gamma_R + 1)^2 + \gamma_X^2}}, \tag{76}$$

and

$$\tan\phi_R = \frac{2\gamma_X}{\gamma_R^2 + \gamma_X^2 - 1}. \tag{77}$$

To compute the probability distribution function for ϕ, $P_\phi(\phi)$, we note that, since ψ is uniformly distributed on any interval of 2π, we can just as well take ψ', which differs from ψ by a constant shift, to be uniformly distributed. Consequently, we have

$$P_\phi(\phi) = \frac{1}{2\pi}\left|\frac{d\psi'}{d\phi}\right|$$
$$= \frac{1}{2\pi}\frac{1}{1 + |\rho_R|^2 - 2|\rho_R|\cos(\phi - \phi_R)}. \tag{78}$$

Thus $P_\phi(\phi)$ is peaked at the angle ϕ_R corresponding to the phase angle of the free space reflection phase, with a degree of peaking that depends on $|\rho_R|$, the magnitude of the free space reflection coefficient. 'Perfect matching' corresponds to $\gamma_R = 1$, $\gamma_X = 0$, and $|\rho_R| = 0$, in which case $P_\phi(\phi)$ is uniform.

We next consider the case of poor matching for which $|\rho_R| \cong 1$ and $P_\phi(\phi)$ is strongly peaked at ϕ_R. This behavior can be understood in the context of the frequency dependence of the phase for a given realization. It follows from (73) and (42) that the phase ϕ decreases by 2π as k^2 increases by the spacing between eigenvalues. If $|\rho_R| \cong 1$, then for most of the frequencies in this interval, the phase is near ϕ_R. However, for the small range of frequencies near a resonance, the phase will jump by 2π as the resonance is passed. This indicates that the mode of the cavity is poorly coupled to the transmission line. In the case of good matching, $|\rho_R| = 0$, all phases are equally likely indicating that as a function of frequency the rate of increase of phase is roughly constant. This implies that the resonances are broad, and the cavity is well coupled to the transmission line.

In order to describe the different coupling strengths, we consider the parameter g originally introduced by Fyodorov and Sommers [35] :

$$g = \frac{1 + |\langle e^{j\phi}\rangle|^2}{1 - |\langle e^{j\phi}\rangle|^2}. \tag{79}$$

Evaluating $\langle S \rangle$ using Eq. (78),

$$g = \frac{1 + |\rho_R|^2}{1 - |\rho_R|^2}. \tag{80}$$

Thus, g has a minimum value of 1 in the perfectly matched case and is large if the matching is poor, $|\rho_R| \sim 1$. An analogous quantity is the voltage standing wave ratio on the transmission line when the cavity impedance is set equal to the radiation impedance,

$$\text{VSWR} = \frac{1 + |\rho_R|}{1 - |\rho_R|} = g + \sqrt{g^2 - 1}. \tag{81}$$

To test Eq. (78), we compared its predictions for the phase distribution with direct numerical calculations obtained using HFSS (High Frequency Structure Simulator) for the case of the cavity
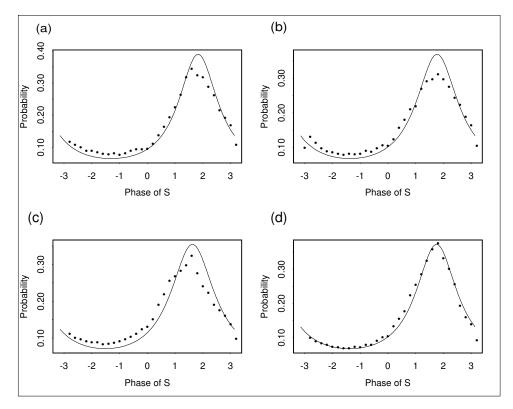
FIG. 11: Histogram of the reflection phase distribution for an HFSS calculation for the cavity in Fig. 3 with center frequencies located at (a) 7GHz, (b) 7.5GHz, (c) 8GHz, (d) 8.5GHz, and with sweeping span equal to 0.1GHz. Numerical data are compared with Eq. (78) using parameters determined by Z_R at the corresponding center frequencies.

and coupling detail as specified in Fig. 6. As compared to what was done for Fig. 6, we have narrowed the frequency range to 0.1 GHz bands for each realization in 1000 10^{-4} GHz steps centered at 7 GHz, 7.5 GHz, 8 GHz, 8.5 GHz. Instead of calculating the radiation impedance for every frequency, we use the value of Z_R at the middle frequency of the interval in calculating the values of γ_R and γ_X. We present theoretical phase density distribution functions together with numerical histogram results in Fig. 11. The agreement between the theory, Eq. (78), and the numerical results is surprisingly good, especially considering the rather small (0.1GHz) frequency range used.

B. Multiple Ports

We now consider the multiport case. We first study the influence of mismatch $\gamma_R \neq 1$, $\gamma_X \neq 0$ in the two-port case; then we study situations with more than two ports, but with perfect coupling ($\gamma_R = 1, \gamma_X = 0$); finally we generalize our results to multi-port non-perfect coupling.

41

1. Two-port case

We recall that for TRS systems the reactance matrix X is real and symmetric, and can be diagonalized by an orthogonal matrix O, Eq. (63). If identical ports are connected to identical transmission lines of characteristic impedance Z_0, then the scattering matrix S is also diagonalized by O, and we can write

$$S = O \begin{pmatrix} e^{j\phi_1} & 0 \\ 0 & e^{j\phi_2} \end{pmatrix} O^T. \tag{82}$$

The scattering phases ϕ_1 and ϕ_2 are then related to the eigenvalue angles θ_i by formulas analogous to (73)-(79).

Substituting Eq. (63) for O in (82) and multiplying the matrices, we obtain

$$|S_{11}|^2 = \cos^4 \eta + \sin^4 \eta + 2 \cos^2 \eta \sin^2 \eta \cos(\phi_1 - \phi_2). \tag{83}$$

We can now compute the expected value of the square of $|S_{11}|$ by assuming that η is independent of the angles ϕ_1 and ϕ_2 and is uniformly distributed, which yields $\langle \cos^4 \eta + \sin^4 \eta \rangle = 3/4$, $2\langle \cos^2 \eta \sin^2 \eta \rangle = 1/4$ and

$$\langle |S_{11}|^2 \rangle = \frac{3}{4} + \frac{1}{4} \langle \cos(\phi_1 - \phi_2) \rangle. \tag{84}$$

Assuming the angles θ_1 and θ_2 are distributed according to Eq. (60) and using the relation between $\phi_{1,2}$ and $\theta_{1,2}$, evaluation of $\langle \cos(\phi_1 - \phi_2) \rangle$ is carried out in Appendix D. The result is

$$\langle |S_{11}|^2 \rangle = 1 - \frac{1 - |\rho_R|^4}{8|\rho_R|^2} - \frac{(1 - |\rho_R|^2)^3}{16|\rho_R|^3} \ln \frac{1 - |\rho_R|}{1 + |\rho_R|}. \tag{85}$$

A plot of $\langle |S_{11}|^2 \rangle$ versus $|\rho_R|$ is shown in Fig. 12(a). Also shown are data points obtained by taking 10^6 realizations of the impedance matrix (58) and computing the average of $|S_{11}|^2$ for different combinations of γ_R and γ_X characterizing the radiation impedance. The data confirm that the average of $|S_{11}|^2$ depends only on the magnitude of the free space reflection coefficient (76) and not its phase (77).

In the TRSB case, the eigenvalues of the X matrix are still real, but the eigenvectors are complex. In this case, Eq. (82) is replaced by

$$S = U \begin{pmatrix} e^{j\phi_1} & 0 \\ 0 & e^{j\phi_2} \end{pmatrix} U^\dagger, \tag{86}$$

where the unitary matrix U is given by Eq. (64). Multiplying the matrices in Eq. (86), we find the same expression for $|S_{11}|^2$, Eq. (83), as in the TRS case. The average of $|S_{11}|^2$ will be different in the

TRSB case because of the different statistics for η, θ_1 and θ_2 which characterize the eigenfunctions and eigenvalues of the impedance matrix. In particular, η has a distribution, arising from the SU(2) group [37],

$$P_\eta(\eta) = |\sin(2\eta)|, \tag{87}$$

which yields $\langle \cos^4 \eta + \sin^4 \eta \rangle = 2/3$, $2\langle \cos^2 \eta \sin^2 \eta \rangle = 1/3$, thus,

$$\langle |S_{11}|^2 \rangle = \frac{2}{3} + \frac{1}{3} \langle \cos(\phi_1 - \phi_2) \rangle. \tag{88}$$

Recalling that θ_1 and θ_2 are distributed according to (60) with $\beta = 2$, this results in a different set of integrals (see Appendix D). The result is

$$\langle |S_{11}|^2 \rangle = 1 - \frac{(|\rho_R|^2 - 1)(|\rho_R|^2 - 3)}{6}, \tag{89}$$

which depends only on the magnitude of the free space reflection coefficient. A plot of $\langle |S_{11}|^2 \rangle$ from Eq. (89) versus $|\rho_R|$ is also shown in Fig. 12(a), along with data point obtained by taking 10^6 realizations of the TRSB impedance matrix (58) and computing the average of $|S_{11}|^2$ for different combinations of γ_R and γ_X characterizing the free space impedance. Once again, the data collapse to the curve predicted in Eq. (89).

We now test the relation between $\langle |S_{11}|^2 \rangle$ and $|\rho_R|$ with the impedance matrices we obtained from HFSS two-port calculations. We can vary the transmission line impedance Z_0 and generate $\langle |S_{11}|^2 \rangle$ and $|\rho_R|$. However, the range of $|\rho_R|$ values accessible doing this is limited because of the large inductive radiation reactance associated with the coupling port. To extend the range of $|\rho_R|$ we add a shunt conductance $Y = (j\omega C)$ in parallel with each port. This results in a modified cavity impedance matrix $Z'_{cav} = (Z_{cav}^{-1} + j\omega C \tilde{1})^{-1}$. We then form the scattering matrix

$$S = (Z'_{cav} + Z_0)^{-1}(Z'_{cav} - Z_0). \tag{90}$$

The corresponding free space reflection coefficient is generated by $Z'_R = (Z_R^{-1} + j\omega C)^{-1}$ and $|\rho_R| = |Z'_R + Z_0|^{-1}|Z'_R - Z_0|$. By choosing appropriate combinations of ωC and Z_0, we can achieve a range of $|\rho_R|$ values between 0 and 1. For each $|\rho_R|$ value, we average $|S_{11}|^2$ over frequencies and realizations and plot the points on Fig. 12(b). These compare favorably with the theoretical curve based on the random matrix theory results.

We have also generated histograms of $|S_{11}|^2$ for both the TRS and TRSB cases using our Random Coupling Model in the perfectly matched case $|\rho_R| = 0$. As shown in Fig. 13, these agree well with those generated directly from ϕ_1 and ϕ_2 according to Eq. (60) and η appropriately distributed as discussed previously.
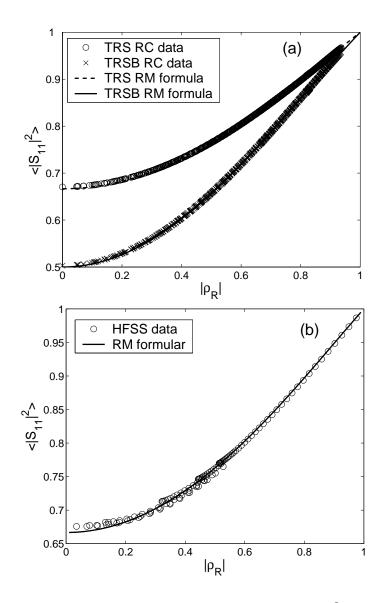
FIG. 12: (a) Numerical simulation for the average reflection coefficient $\langle |S_{11}|^2 \rangle$ vs $|\rho_R|$ defined in Eq. (76) for the TRS and the TRSB system, taking 10^6 realization of the impedance matrix, 30 uniformly spaced values of γ_R from 0.1 to 3, and 31 equally spaced values of γ_X from 0 to 3. (b) Average reflection coefficient $\langle |S_{11}|^2 \rangle$ vs $|\rho_R|$ using the cavity impedance and radiation impedance from HFSS calculation and varying the values of Z_0 and the capacitive reactance Y

2. M-port Case, $M > 2$

Using the random coupling model (58) and assuming perfect coupling $\gamma_R = 1$, $\gamma_X = 0$ (i.e. $|\rho_R| = 0$), we have simulated the S matrix for cases of two to seven ports. The results for the
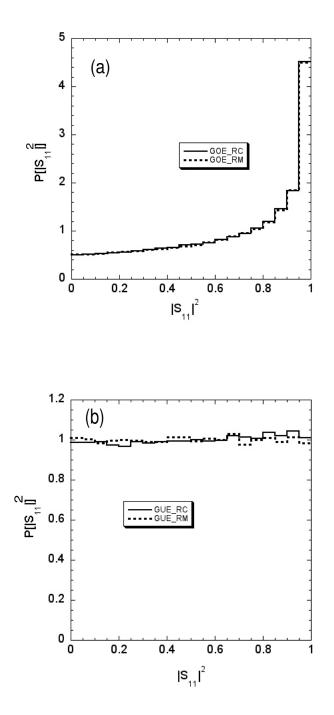
FIG. 13: Histogram of reflection coefficient in (a) TRS and (b) TRSB systems, where the solid curve is generated from our Random Coupling Model, and the dash curve is generated directed from the joint pdf of ϕ_1 and ϕ_2 from Eq. (60).

average reflection and transmission coefficients were found to satisfy:

$$\text{TRS}: \qquad \langle |S_{ij}|^2 \rangle = \begin{cases} \frac{2}{M+1} & i = j, \\[2mm] \frac{1}{M+1} & i \neq j, \end{cases} \tag{91}$$

and

$$\text{TRSB}: \qquad \langle |S_{ij}|^2 \rangle = \begin{cases} \frac{1}{M} & i = j, \\[2mm] \frac{1}{M} & i \neq j, \end{cases} \tag{92}$$

where M is the number of ports connecting the cavity to transmission lines. It seems that, in the TRS case, the input waves "remember" their entry port and have a preference for reflection through it (this is related to the concept of "weak localization" reviewed in [38]). In contrast, for the TRSB case, the waves behave as if they forget through which port they entered the chaotic cavity, and thus all the ports have equal probability of being the output for the waves.

We now briefly discuss the multiport case with $M > 2$ and with mismatch ($|\rho_R| > 0$). As long as the assumption that the eigenfunctions (η) and the eigenvalues (θ or ϕ) are independent is still true, $\langle |S_{11}|^2 \rangle$ is related to the mismatch only through $\langle \cos(\phi_k - \phi_l) \rangle$, similar to the expression in Eq. (84). The same series steps specified in Appendix C can be carried out to show that $\langle \cos(\phi_k - \phi_l) \rangle$, as well as $\langle |S_{11}|^2 \rangle$, depend only on $|\rho_R|$ (and are independent of the phase of ρ_R). We have verified this by numerical simulation using the impedance matrix generated from the Random Coupling Theory (58) with up to seven channels.

VIII.   SUMMARY

We have applied the concepts of wave chaos to the problem of characterizing the impedance and scattering matrices for irregular electromagnetic cavities in the small wavelength regime. The coupling of energy in and out of ports in such cavities depends on both the geometry of the port and the geometry of the cavity. We have found that in a statistical treatment these effects can approximately be separated. The geometry of the port is characterized by its radiation impedance which has both a real and imaginary part. This impedance describes the port in the case in which the distant walls of the cavity are treated as perfect absorbers. The effects of geometry of the cavity can be treated in a statistical way using the random coupling model introduced in this paper.

The random coupling model is expressed most generally for lossless cavities by Eq. (56). To use this model one needs to know the radiation resistance matrix describing the ports, the size of

the cavity, which determines the average density of eigenstates Δ, and whether the waves in the cavity satisfy time reversal symmetry (TRS) or not (TRSB). This last condition determines the statistical properties of the eigenvalue spacings, $k_{n+1}^2 - k_n^2$, and coupling strengths, w_n. The effect of distributed losses can also be incorporated in the random coupling model.

The random coupling model predicts that in the identical port case eigenvalues of the impedance matrix are Lorentzian distributed with a mean equal to the radiation reactance and a width equal to the radiation resistance. The correlation between eigenvalues and eigenvectors is found to be the same as in random matrix theory.

The Lorentzian prediction is tested by direct numerical solution of Maxwell's equation for the cavity of Fig. 3. The predictions are verified if an additional averaging over frequency is introduced. Absent this averaging, there are systematic variations in the mean reactance which need further investigation.

Acknowledgments

APPENDIX A: EVALUATION OF THE MEAN REACTANCE, EQ. (40)

In this appendix we derive the radiation impedance corresponding to the current distribution profile $u(x,y) = \pi^{-1}\delta(x^2 + y^2 - a^2)$. Inserting this function into Eq. (23) and Fourier transforming in x and y with transform variable $\vec{k}_n$ we have

$$(k^2 - k_n^2)\bar{V}_T(\vec{k}_n) = -jkh\eta_0 \hat{I} \int d^2\vec{r}\, \frac{\delta(r-a)}{2\pi a} e^{-j\vec{k}_n \cdot \mathbf{r}} \tag{A1}$$

where $\bar{V}_T(\vec{k}_n)$ is the Fourier transform of $\hat{V}_T$. The right hand side of (A1) can be evaluated in cylindrical coordinates making use of the identity,

$$\int_0^{2\pi} \frac{d\phi}{2\pi} e^{-jk_n a \cos\phi} = J_0(k_n a). \tag{A2}$$

The result is,

$$\bar{V}_T(\vec{k}_n) = -\frac{jkh\eta_0 J_0(k_n a)}{k^2 - k_n^2}\hat{I}. \tag{A3}$$

The port voltage is given by Eq. (24) and may be evaluated using Parseval's theorem,

$$\hat{V} = \int d^2\vec{r}\, u(\vec{r})\hat{V}_T(\vec{r}) = \int \frac{d^2\vec{k}_n}{(2\pi)^2} \hat{V}_T(\vec{k}_n) J_0(k_n a), \tag{A4}$$

where $d^2\vec{k}_n = d\phi\, k_n dk_n$ and ϕ is the angle of $\vec{k}_n$. This gives $\hat{V} = Z_R \hat{I}$ where

$$Z_R = -jkh\eta_0 \int \frac{d^2\vec{k}_n}{(2\pi)^2} \frac{J_0^2(k_n a)}{k^2 - k_n^2}. \tag{A5}$$

This has the form of Eq. (34) if we identify

$$R_R(k_n) = \frac{kh\eta_0}{4} J_0^2(k_n a) \tag{A6}$$

as the radiation resistance.

An alternate evaluation of this same quantity can be made by solving Eq. (23) exploiting the fact that the current source is cylindrically symmetric. We find

$$\hat{V}_T = A J_0(k_n a) \quad r < a, \tag{A7}$$

and

$$\hat{V}_T = B H_0^{(2)}(k_n a) \quad r > a, \tag{A8}$$

where $H_0^{(2)}$ is the Hankel function of the second kind, and corresponds to outgoing waves at infinity for our choice of tie dependence ($e^{j\omega t}$). Applying the conditions of continuity of $\hat{V}_T$ at $r = a$ and the jump condition obtained by integrating Eq. (23) from $r = a - \epsilon$ to $r = a + \epsilon$,

$$\lim_{\epsilon \to 0^+} \left\{ a\frac{\partial \hat{V}_T}{\partial r}(r = a + \epsilon) - a\frac{\partial \hat{V}_T}{\partial r}(r = a - \epsilon) \right\} = -\frac{jkh\eta_0 \hat{I}}{2\pi}, \tag{A9}$$

we find $\hat{V}_T(a) = Z_R\hat{I}$ where

$$Z_R = -\frac{jkh\eta_0}{2\pi ka}\frac{H_0^{(2)}(ka)J_0(ka)}{W(ka)} \tag{A10}$$

and W is the Wronskian,

$$W(ka) = J_0(ka)H_0^{(2)'}(ka) - J_0'(ka)H_0^{(2)}(ka) = -2j/(\pi ka). \tag{A11}$$

Representing the Hankel function in terms of the Bessel functions of the first and second kind $H_0^{(2)} = J_0 - jY_0$, we have

$$Z_R = \frac{kh\eta_0}{4}[J_0^2(ka) - jY_0(ka)J_0(ka)]. \tag{A12}$$

Comparison of (A5) and(A11) leads to Eq. (40).

APPENDIX B: LORENTZIAN DISTRIBUTION FOR ξ

In this appendix we discuss the probability density distribution for ξ in Eq. (42)

$$\xi = \sum_{n=1}^{N} \eta_n, \tag{B1}$$

where $\eta_n = -w_n^2/[\pi(k^2 - k_n^2)]$ and we have dropped the superscribed tilde on the notation for the normalized wavenumber. In Eq. (B1) the w_n are Gaussian random variables with zero mean and unit variance, and, for a Poisson level distribution, each of the values k_n^2 are independently uniformly distributed in the interval $[0, N]$. This prescription maintains the mean spacing between k_n^2 values at unity. With this assumption on the statistics of k_n^2 and w_n the variables η_n are independent and identically distributed. Therefore, $P_\xi(\xi)$, the probability density function of ξ, is

$$P_\xi(\xi) = \int d\eta_1 .. d\eta_N \delta(\xi - \sum_n \eta_n) \prod_{i=1}^{N} P_\eta(\eta_i). \tag{B2}$$

We will investigate the characteristic function of the random variable ξ, i.e. the Fourier transformation of $P_\xi(\xi)$,

$$\bar{P}_\xi(t) = \int d\eta_1 .. d\eta_N e^{-jt \sum_n \eta_n} \prod_{i=1}^{N} P_\eta(\eta_i) = [\bar{P}_\eta(t)]^N, \tag{B3}$$

where

$$
\begin{aligned}
\bar{P}_\eta(t) &= \int d\eta e^{-jt\eta} P_\eta(\eta) \\
&= \int_{-\infty}^{\infty} dw \frac{1}{\sqrt{2\pi}} exp(-\frac{w^2}{2}) \int_0^N \frac{dk_n^2}{N} \int d\eta e^{-jt\eta} \delta[t - \frac{w^2/\pi}{k^2 - k_n^2}] \\
&= \int_0^N \frac{dk_n^2}{N} \frac{1}{[1 + 2j\frac{t}{\pi}\frac{1}{k^2 - k_n^2}]^{-\frac{1}{2}}}.
\end{aligned}
\tag{B4}
$$

Note that $\bar{P}_\eta(-t) = \bar{P}_\eta^*(t)$ from the reality condition, so it is sufficient to evaluate the integral above for the case of positive t.

The integrand in (B4) has singularities of $k_n^2 = k^2$ and $k_n^2 = k^2 + 2jt/\pi$. The integration contour (defined to be along the real k_n^2 axis) passes through the singularity at $k_n^2 = k^2$. However, this singularity is weak, $(k^2 - k_n^2)^{1/2}$, and we can regard the contour as passing below the singularity. Thus, for $t > 0$ we may deform the integration contour into a large semicircle in the lower half k^2 plane starting at $k_n^2 = 0$ and ending at $k_n^2 = N$. For each point on this contour $2t/[\pi(k_n^2 - k^2)]$ is small and we can Taylor expand the integrand for $|k_n^2 - k^2| \sim N$

$$
\begin{aligned}
\bar{P}_\eta(t) &= \frac{1}{N} \int_0^N dk_n^2 [1 - \frac{j}{2} \frac{2t}{\pi(k_n^2 - k^2)}] + O(\frac{t^2}{N^2}) \\
&= 1 - \frac{t}{N} - j\frac{t}{\pi N} \log|\frac{N - k^2}{k^2}| + O(t^2/N^2).
\end{aligned}
\tag{B5}
$$

The sign of the term $-t/N$ is determined by deforming the contour into the lower half plane below the pole $k_n^2 = k^2$. In the limit of $N \to \infty$ we may drop the term $O(t^2/N^2)$. Also, recalling the reality condition $\bar{P}_\eta(-t) = \bar{P}_\eta^*(t)$, (B5) yields

$$\bar{P}_\eta(t) \cong 1 - \frac{|t|}{N} - j\frac{t}{\pi N}\log\left|\frac{N - k^2}{k^2}\right|, \tag{B6}$$

Therefore, $\bar{P}_\xi(t)$ is:

$$\begin{aligned}\bar{P}_\xi(t) &= [1 - \frac{|t|}{N} - j\frac{t}{\pi N}\log\left|\frac{N - k^2}{k^2}\right|]^N \\ &= \exp[-|t| - j\frac{t}{\pi}\log\left|\frac{N - k^2}{k^2}\right|].\end{aligned} \tag{B7}$$

Taking the inverse Fourier transform in t we find that ξ is a Lorentzian distributed random variable with unit characteristic width and a mean value $\log|(N - k^2)/k^2|/\pi$.

APPENDIX C: VARIANCE OF CAVITY REACTANCE AND RESISTANCE IN THE LOSSY CASE.

From Eq. (68), we obtain the expression for the complex impedance in the single part case,

$$Z(\sigma) = \frac{1}{\pi} \sum_{1}^{N} [\frac{\Delta(k_n^2) R_R(k_n^2) w_n^2 [k_d^2 + j(k_n^2 - k^2)]}{(k^2 - k_n^2)^2 + (k_d^2)^2}]$$

$$= R(\sigma) + jX(\sigma),$$

(C1)

where Δ is the mean spacing $\langle k_n^2 - k_{n-1}^2 \rangle$, $X(\sigma)$ and $R(\sigma)$ are cavity reactance and resistance in the lossy case and $k_d^2 = k^2 \sigma$. In this section, we are going to evaluate the mean and variance of $X(\sigma)$ and $R(\sigma)$ as well as their covariance.

We first investigate the mean of $R(\sigma)$.

$$E[R(\sigma)] = \frac{1}{\pi} \int \ldots \int dk_1^2 \ldots dk_N^2 P_J(k_1^2, \ldots, k_N^2) \sum_{n'=1}^{N} \frac{R_R \Delta \langle w_{n'}^2 \rangle k_d^2}{(k^2 - k_{n'}^2)^2 + k_d^4},$$

(C2)

where P_J is the joint distribution of eigenlevels $(k_1^2, \ldots, k_N^2)$ assuming they are unordered. Since the levels are not ordered, in each term of the sum, we can integrate over all $k_n^2 \neq k_{n'}^2$, and obtain N identical terms. Thus,

$$E[R(\sigma)] = \frac{N}{\pi} \int dk_{n'}^2 P_1(k_1^2) R_R \Delta \langle w^2 \rangle \frac{k_d^2}{(k^2 - k_{n'}^2)^2 + k_d^4}$$

(C3)

where $P_1(k_{n'}^2)$ is distrubtion for a single level. Here we have introduced an integer N representing the total number of levels. We will take the limit of $N \to \infty$. The single level probability distribution then satisfies by definition,

$$P_1(k_{n'}^2) = \frac{1}{N \Delta(k_{n'}^2)}.$$

(C4)

We next assume that the radiation resistance $R_R(k_{n'}^2)$ is relatively constant over the interval of $k_{n'}^2$ values satisfying $|k_n^2 - k_{n'}^2| < k_d^2$ and we will move it outside the integral replacing it by $R_R(k^2)$. Assuming that $k^2 \sigma$ is not too large we can take the end points at the integral to plus and minus infinity and evaluate Eq. (C3) as

$$E[R] = \frac{R_R}{\pi} \int_{-\infty}^{\infty} dx \frac{1}{x^2 + 1} = R_R(k^2),$$

(C5)

where $x = (k_{n'}^2 - k^2)/k_d^2$. Thus the expected value of the real part of cavity impedance is the radiation resistance independent of the amount of damping. This is somewhat surprising since we have previously asserted that in the lossless case, the cavity resistance is zero. The constancy of

the expected resistance results from the resonant nature of the cavity impedance. When losses are small $k^2\sigma \ll 1$ for almost all frequencies the resistance is small however for the small set of the frequencies near a resonance the resistance is large. This is evedent in the histograms of Fig. (10b).

In order to obtain the variance of $R(\sigma)$, we calculate the second moment of $R(\sigma)$,

$$E[R(\sigma)^2] = (\frac{1}{\pi})^2 \int \ldots \int dk_1^2 \ldots dk_N^2 P_J(k_1^2,\ldots,k_N^2) \sum_{n',m'=1}^{N} \frac{\Delta^2 R_R(k_{n'}^2)R_R(k_{m'}^2)\langle w_{m'}^2 w_{n'}^2\rangle k_d^4}{((k^2 - k_{m'}^2)^2 + k_d^4)((k^2 - k_{n'}^2)^2 + k_d^4)}$$

$$= I_1 + I_2.$$
(C6)

Following the arguments advanced to calculate $E[R(\sigma)]$, we note that there will be N terms in the double sum for which $k_{n'}^2 = k_{m'}^2$ giving

$$I_1 = \frac{N}{\pi^2} \int dk_{n'}^2 P_1(k_{n'}^2) \frac{\Delta^2 R^2(k_{n'}^2)\langle w_{n'}^4\rangle k_d^4}{[(k^2 - k_{n'}^2)^2 + k_d^4]^2}$$
(C7)

and $N(N-1)$ terms for which $k_{m'}^2 \neq k_{n'}^2$ giving

$$I_2 = N(N-1) \iint dk_{n'}^2 dk_{m'}^2 \frac{P_2(k_{n'}^2, k_{m'}^2)\Delta(k_{n'}^2)\Delta(k_{m'}^2 R_R(k_{n'}^2)R_R(k_{m'}^2)\langle w_{n'}^2\rangle\langle w_{m'}^2\rangle k_d^4}{[(k^2 - k_{n'}^2)^2 + k_d^4][(k^2 - k_{m'}^2)^2 + k_d^4]}.$$
(C8)

For the first integral we use (C4) for the single level distribution function, and making the smae approximation as before, we obtain

$$I_1 = R_R^2(k^2)\frac{\langle w^4\rangle\Delta(k^2)}{2\pi k_d^2}.$$
(C9)

For the second integral we need to introduce the two level distribution function. For the spectra that we consider, the two level distribution has the form

$$P_2(k_{n'}^2, k_{m'}^2) = (\frac{1}{N\Delta})^2[1 - g(|k_{n'}^2 - k_{m'}^2|)].$$
(C10)

Here the function g describes the correllations between two energy levels. For uncorrellated levels giving a Poisson distribution of spacings we have $g = 0$. In the presence of level repulsion we expect $g(0) = 1$ with $(1 - g) \propto |k_{n'}^2 - k_{m'}^2|^\beta$ for small spacing, and $\beta = 1$ for TRS and $\beta = 2$ for TRSB systems. As $|k_{n'}^2 - k_{m'}^2| \to \infty$, $g \to 0$ indicating loss of correlation for two widely separated levels. The function g will be different for spectra produced by random matrices and spectra genergated from sequences of independent spacings. Expressions of g for the spectra of random matrices can be found in the book by Mehta ([18], Ch. 5 & 6). We will get an insight for the expression for g for spectra generated by sequences of independent spacings later in this appendix.

Based on expression (C10) and the usual assumptions on the slow variations of R_R and Δ with eigenvalue $k_{n'}^2$ we obtain

$$I_2 = (E[R])^2 - I_g,$$
(C11)

where the first term comes from the 1 in C10 and the second term comes from the correlation function g

$$I_g = \frac{R_R(k^2)\langle w^2 \rangle^2}{\pi} \int_{-\infty}^{\infty} \frac{d\tilde{k}^2}{k_d^2} \frac{2}{4 + (\tilde{k}^2/k_d^2)^2} g(|\tilde{k}^2|).$$

(C12)

The variance of R is thus given by

$$Var[R] = E[R]^2 - E[R^2]$$
$$= R_R^2 \frac{\Delta}{k_d^2} [\frac{\langle w^4 \rangle}{2\pi} - \frac{\langle w^2 \rangle^2}{\pi} \int_{-\infty}^{\infty} \frac{d\tilde{k}^2}{\Delta} \frac{2g(|\tilde{k}^2|)}{4 + (\tilde{k}^2/k_d^2)^2}].$$

(C13)

Note, since w is a Gaussian random variable with zero mean and unit variance, $\langle w^2 \rangle = 1$ and $\langle w^4 \rangle = 3$.

Equation (C13) shows that the variances of R depends on k_d^2/Δ, the ratio of the damping width to the mean spacing of eigenvalues. In the low damping case, $k_d^2/\Delta \ll 1$, the integrand in (C13) is dominated by the values of $|\tilde{k}^2| < \Delta$ and we replace g by its value $g(0)$. Doing the integral we find

$$Var[R] = R_R^2 [\frac{\Delta}{k_d^2} \frac{\langle w^4 \rangle}{2\pi} - g(0)\langle w^2 \rangle^2].$$

(C14)

Since the damping is small, the first term dominates and the variance is independent of the eigenvalue correlation function. This is consistent with our previous findings. In the high damping limit, $k_d^2 > \Delta$, the integral in (C13) is dominated by $\tilde{k}^2$ values of order Δ and we have,

$$Var[R] = R_R^2 \frac{\Delta}{k_d^2} [\frac{3}{2\pi} - \frac{1}{\pi} \int_0^{\infty} \frac{d\tilde{k}^2}{\Delta} g(|\tilde{k}^2|)].$$

(C15)

The variance decreases as damping increases with a coefficient that depends on the correlation function. Physically the correlations are important because in the high damping case a relatively large number of terms in the sum (C1) contribute to the impedance and the sum is sensitive to correlations in these terms.

The integral of the correlation function can be evaluated for different spectra. For spectra generated from random matrices, we have

$$g(e) = s(e)^2 - \frac{\partial s}{\partial e}[(\int_0^e de' s(e')) - \frac{1}{2} sgn(e)]$$

(C16)

for TRS matrices and

$$g(e) = s(e)^2$$

(C17)

for TRSB matrices, where $e = \tilde{k}^2/\Delta$. In both cases, we find

$$\int_0^{\infty} deg(e) = \frac{1}{2}.$$

(C18)

However, to consider the TRSB case we need to repeat the calculation including complex values of the Gaussian variable w. The result is

$$Var[R(\sigma)] = \frac{R_R^2}{\pi}\frac{\Delta}{k_d^2}[1 - \int_0^\infty \frac{d\tilde{k}^2}{\Delta}g(|\tilde{k}^2|)]$$ (C19)

For spectra generated by sequences of independent spacing distributions we will show

$$\int_0^\infty \frac{d\tilde{k}^2}{\Delta}g(|\tilde{k}^2|) = 1 - \frac{1}{2}\langle s^2\rangle$$ (C20)

where $\langle s^2\rangle$ is the expected value fo the nearest neighbor spacing squared. This gives

$$\int_0^\infty \frac{d\tilde{k}^2}{\Delta}g(|\tilde{k}^2|) = \begin{cases} 1 - \frac{2}{\pi} & \text{for TRS,} \\ 1 - \frac{3\pi}{16} & \text{for TRSB.} \end{cases}$$ (C21)

Note also that (C20) gives the required value of zero for Poisson spacing distributions.

We now derive the g-integral for spectra generated from independent spacings. We introduce a conditional distribution $P_m(s)$ that is the probability density that the mth eigenvalue is in the range of $[s,\ s+ds]$ given that eigenvalue at zero. When $m = 1$, $P_1(s)$ is reduced to spacing distribution $p(s)$. For convenience, here s is the normalized spacing with unit mean. Thus, $1 - g(s)$ stands for the probability that there exists an eigenlevel at [s, s+ds] given one level located at 0, which naturally can be expressed as the summation of $P_m(s)$,

$$\begin{aligned} 1 - g(s) &= \sum_{m=1}^\infty P_m(s) \\ &= \sum_{m=1}^\infty [\int \prod_{i=1}^m ds_i P_1(s_i)\delta(s - \sum_{i=1}^m s_i)]. \end{aligned}$$ (C22)

Doing Laplace transformation to both sides of Eq. (C22), it yields

$$\frac{1}{\tau} - \int_0^\infty dse^{-\tau s}g(s) = \sum_{m=1}^\infty [\bar{P}_1(\tau)]^m = \frac{\bar{P}_1(\tau)}{1 - \bar{P}_1(\tau)}.$$ (C23)

Because for small value of τ,

$$\begin{aligned} \bar{P}_1(\tau) &= \int_0^\infty e^{-s\tau}P_1(s)ds \\ &\sim \int_0^\infty (1 - s\tau + \frac{s^2\tau^2}{2})P_1(s)ds \\ &= 1 - \tau\langle s\rangle + \frac{\tau^2}{2}\langle s^2\rangle, \end{aligned}$$ (C24)

we can approximate the integration of $g(s)$ to be

$$\begin{aligned} \int_0^\infty dsg(s) &= \lim_{\tau\to 0}\int_0^\infty dse^{-\tau s}g(s) \\ &= \lim_{\tau\to 0}[\frac{1}{\tau} - \frac{\bar{P}_1(\tau)}{1 - \bar{P}_1(\tau)}] \\ &= 1 - \frac{1}{2}\langle s^2\rangle \end{aligned}$$ (C25)

Put it back into the Eq. (C15), we finally express the variance of $R(\sigma)$ in term of the lossy parameter and spacing distribution,

$$Var[R(\sigma)] = R_R^2 \frac{\Delta}{k_d^2} (\frac{\langle w^4 \rangle}{2\pi} - \frac{\langle w^2 \rangle^2}{\pi} (1 - \frac{1}{2} \langle s^2 \rangle)).$$ (C26)

Similar process can be carried out to get the variance of $X(\sigma)$ as well as the covariance of $R(\sigma)$ and $X(\sigma)$:

$$Var[X(\sigma)] = Var[R(\sigma)], \qquad Cov[R(\sigma), X(\sigma)] = 0.$$ (C27)

APPENDIX D: EVALUATION OF $\langle |S_{11}|^2 \rangle$

In this appendix, we will start from the one-port case, and obtain an expression for the phase of S in term of the reflection coefficient ρ_R defined in Eq. (75). Then, using Eq. (60), we can evaluate $\langle \cos(\phi_1 - \phi_2) \rangle$ for the two-port in the TRS and TRSB cases.

In the one-port case, S can be expressed as

$$
\begin{aligned}
S = e^{j\phi} &= \frac{Z - Z_0}{Z + Z_0} \\
&= \frac{j(\gamma_X + \tilde{\xi}\gamma_R) - 1}{j(\gamma_X + \tilde{\xi}\gamma_R) + 1},
\end{aligned}
\tag{D1}
$$

where $\tilde{\xi}$ is a zero mean, unit width, Lorentzian random variable, which can be written as,

$$
\tilde{\xi} = \tan \theta
\tag{D2}
$$

with θ uniformly distributed in $[-\pi/2, \ \pi/2]$. Putting Eq. (D2) into Eq. (D1), we get

$$
e^{j\phi} = \frac{(\gamma_R + j\gamma_X - 1)e^{j\theta} - (\gamma_R - j\gamma_X + 1)e^{-j\theta}}{(\gamma_R + j\gamma_X + 1)e^{j\theta} - (\gamma_R - j\gamma_X - 1)e^{-j\theta}}.
\tag{D3}
$$

Introducing ρ_R such that

$$
\gamma_R + j\gamma_X - 1 = \rho_R(\gamma_R + j\gamma_X + 1),
\tag{D4}
$$

and defining

$$
e^{-j\alpha} = \frac{\gamma_R - j\gamma_X + 1}{\gamma_R + j\gamma_X + 1},
\tag{D5}
$$

we obtain a compact expression for ϕ in term of θ and ρ_R,

$$
\begin{aligned}
e^{j\phi} &= \frac{\rho_R - e^{-j(2\theta + \alpha)}}{1 - \rho_R^* e^{-j(2\theta + \alpha)}} \\
&= e^{j\phi_R} e^{-j2\theta'} \frac{1 + |\rho_R|e^{j2\theta'}}{1 + |\rho_R|e^{-j2\theta'}},
\end{aligned}
\tag{D6}
$$

where $2\theta' = (2\theta + \alpha + \pi + \phi_R)$. Since α and ϕ_R depend only on the coupling coefficient γ_R and γ_X, and 2θ is uniformly distributed in $[0, \ 2\pi]$, the angle $2\theta'$ is also uniform in $[0, 2\pi]$. Thus,

$$
\begin{aligned}
P_\phi(\phi) &= P_{2\theta'}(2\theta') |\frac{d(2\theta')}{d\phi}| \\
&= \frac{1}{2\pi} \frac{1}{1 + |\rho_R|^2 - 2|\rho_R|\cos(\phi - \phi_R)}.
\end{aligned}
\tag{D7}
$$

The relation between ϕ and $2\theta'$ also holds true for multi-port cases. Furthermore, from the joint probability density function of $2\theta_1$ and $2\theta_2$ in Eq. (60), which is only a function of the difference of

57

two angles, we find that $2\theta'_1$ and $2\theta'_2$ have the same joint distribution specified in Eq. (60). Thus we can evaluate

$$
\begin{aligned}
\langle \cos(\phi_1 - \phi_2) \rangle &= Re[e^{j\phi_1 - j\phi_2}] \\
&= Re[\frac{e^{-j2\theta'_1} + |\rho_R|}{1 + |\rho_R|e^{-j2\theta'_1}} \frac{e^{j2\theta'_2} + |\rho_R|}{1 + |\rho_R|e^{j2\theta'_2}}],
\end{aligned}
\tag{D8}
$$

by using the joint distribution of $2\theta'_1$ and $2\theta'_2$, $P_\beta(2\theta_1, 2\theta_2) \propto |e^{j2\theta'_1} - e^{j2\theta'_2}|^\beta$, where $\beta = 1$ corresponds to the TRS case, and $\beta = 2$ for TRSB case.

Introducing $\psi_1 = 2\theta'_1$, $\psi_2 = 2\theta'_2$, and their difference $\psi_- = \psi_1 - \psi_2$, we obtain for the average of $\cos(\phi_1 - \phi_2)$,

$$
\begin{aligned}
\langle \cos(\phi_1 - \phi_2) \rangle &= \iint \frac{d\psi_1 d\psi_2}{(2\pi)^2} P(\psi_1, \psi_2) Re[\frac{e^{-j\psi_1} + |\rho_R|}{1 + |\rho_R|e^{-j\psi_1}} \frac{e^{j\psi_2} + |\rho_R|}{1 + |\rho_R|e^{j\psi_2}}] \\
&= \int \frac{d\psi_-}{2\pi} P(\psi_-) Re[\int_0^{2\pi} \frac{\psi_2}{2\pi} \frac{e^{-j(\psi_- + \psi_2)} + |\rho_R|}{1 + |\rho_R|e^{-j(\psi_- + \psi_2)}} \frac{e^{j\psi_2} + |\rho_R|}{1 + |\rho_R|e^{j\psi_2}}].
\end{aligned}
\tag{D9}
$$

The inner integral can be calculated by introducing a complex variable $z = e^{j\psi_2}$ in terms of which the inner integral becomes

$$
\frac{1}{2\pi j} \oint_{unitcircle} \frac{dz f(z)}{z(z + |\rho_R|e^{-j\psi_-})},
\tag{D10}
$$

where $f(z) = (|\rho_R|z + e^{-j\psi_-})(z + |\rho_R|)/(1 + z|\rho_R|)$. Evaluating this integral via the residues at the two poles within the unit circle, $z = 0$ and $z = -|\rho_R|e^{-j\psi_-}$, we obtain

$$
\langle \cos(\phi_1 - \phi_2) \rangle = \int_0^{2\pi} \frac{d\psi_-}{2\pi} P(\psi_-)[1 - \frac{(1 - |\rho_R|^4)(1 - \cos \psi_-)}{1 + |\rho_R|^4 - 2|\rho_R|^2 \cos \psi_-}].
\tag{D11}
$$

For the TRS case, $P_{\psi_-}(\psi_-) = \pi|\sin(\psi_-/2)|/2$, and Eq. (D11) yields

$$
\langle \cos(\phi_1 - \phi_2) \rangle = \frac{|\rho_R|^4 + 2|\rho_R|^2 - 1}{2|\rho_R|^2} + \frac{(1 - |\rho_R|^2)^3}{4|\rho_R|^3} \ln \frac{1 + |\rho_R|}{1 - |\rho_R|}.
\tag{D12}
$$

For the TRSB case, $P_{\psi_-}(\psi_-) = 2\sin^2(\psi_-/2) = (1 - \cos \psi_-)$, and (D11) yields

$$
\langle \cos(\phi_1 - \phi_2) \rangle = 1 - \frac{(|\rho_R|^2 - 1)(|\rho_R|^2 - 3)}{2}.
\tag{D13}
$$

[1] R. Holland and R. St. John, *Statistical Electromagnetics* (Taylor and Francis, 1999), and references therein.

[2] T. H. Lehman and E. K. Miller, Conference Proceedings: Progress in Electromagnetics Research Symposium, Cambridge, MA, July 1–5, 1991, p. 428.

[3] J. G. Kostas and B. Boverie, IEEE Trans. EMC **33**, 366 (1991).

[4] R. H. Price, H. T. Davis, and E. P. Wenaas, Phys. Rev. E **48**, 4716 (1993).

[5] R. Holland and R. St. John, Conference Proceedings: 10th Annual Review of Progress in Applied Computational Electromagnetics, Monterey, CA, March, 1994, vol. 2, p. 554–568.

[6] D. A. Hill, IEEE Trans. EMC **36**, 294 (1994); **40**, 209 (1998).

[7] L. Cappetta, M. Feo, V. Fiumara, V. Pierro and I. M. Pinto, IEEE Trans. EMC **40**, 185 (1998).

[8] E. P. Wigner, Ann. Math. **53**, 36 (1951); **62**, 548 (1955); **65**, 203 (1957); **67**, 325 (1958).

[9] E. Ott, *Chaos in Dynamical Systems*, second edition (Cambridge University Press, 2002).

[10] M. C. Gutzwiller, *Chaos in Classical and Quantum Mechanics* (Springer-Verlag, 1990).

[11] F. Haake, *Quantum Signatures of Chaos* (Springer-Verlag, 1991).

[12] Y. Alhassid, Rev. Mod. Phys. **72**, 895 (2000); H. U. Baranger and P. A. Mello, Phys. Rev. Lett. **73**, 142 (1994); C. M. Marcus, A. J. Rimberg, R. M. Westervelt, P. F. Hopkins, and A. C. Gossard, Phys. Rev. Lett. **69**, 506 (1992); M. J. Berry, J. A. Katin, R. M. Westervelt, and A. C. Gossard, Phys. Rev. B **50**, 17721 (1994).

[13] H. Weyl, Math. Ann. **77**, 313 (1916).

[14] R. B. Balian and C. Bloch, Ann. Phys. (N.Y.) **60**, 401 (1970); **63**, 592 (1971); **64**, 271 (1971).

[15] R. E. Prange, E. Ott, T. M. Antonsen, B. Georgeot and R. Blumel, Phys. Rev. E **53**, 207 (1996).

[16] M. C. Gutzwiller, J. Math. Phys. **8**, 1979 (1967); **10**, 1004 (1969).

[17] P. So, S. M. Anlage, E. Ott and R. N. Oerter, Phys. Rev. Lett. **74**, 2662 (1995).

[18] M. L. Mehta, *Random Matrices*, second edition (Academic Press, 1991); K. B. Efetov, Adv. Phys. **32**, 53 (1983).

[19] A. D. Mirlin, Phys. Rep. **326**, 260 (2000).

[20] S. W. McDonald and A. N. Kaufman, Phys. Rev. Lett. **42**, 1182 (1979); Phys. Rev. A **37**, 3067 (1988).

[21] O. Bohigas, M. J. Giannoni and C. Schmidt, Phys. Rev. Lett. **52**, 1 (1984).

[22] G. D. Birkhoff, Mathematica **50**, 359 (1927).

[23] H. -J. Stockmann and J. Stein, Phys. Rev. Let. **64**, 2215 (1990).

[24] S. Sridar, Phys. Rev. Lett. **67**, 785 (1991).

[25] E. Ott, Phys. Fluids **22**, 2246 (1979).

[26] M. V. Berry in *Chaotic Behavior of Deterministic Systems. Les Houches Summer School 1981* (North-Holland, 1983).

[27] S. -H. Chung, A. Gokirmak, D. -H. Wu, J. S. A. Bridgewater, E. Ott, T. M. Antonsen and S. M. Anlage, Phys. Rev. Lett. **85**, 2482 (2000).

[28] E. J. Heller, Phys. Rev. Lett. **53**, 1515 (1984).

[29] E. Bogomolny, Physica D **31**, 169 (1988).

[30] M. V. Berry, Proc. Roy. Soc. London Ser. A **423**, 219 (1989).

[31] T. M. Antonsen, E. Ott, Q. Chen, and R. N. Oerter, Phys. Rev. E **51**, 111 (1995).

[32] E. P. Wigner and L. Eisenbud, Phys. Rev. **72**, 29 (1947).

[33] A. M. Lane and R. G. Thomas, Rev. Mod. Phys. **30**, 257 (1958).

[34] C. Mahaux and H. A. Weidenmuller, *Shell-Model Approach to Nuclear Reactions* (North-Holland, Amsterdam, 1969).

[35] Y. V. Fyodorov and H. J. Sommers, J. Math. Phys. **38**, 1918 (1997).

[36] R. A. Jalabert, A. D. Stone and Y. Alhassid, Phys. Rev. Lett. **68**, 3468 (1992).

[37] J. F. Cornwell, *Group Theory in Physics: an Introduction* (Academic Press, San Diego, California, 1997).

[38] P. A. Lee and T. V. Ramakrishnan, Rev. Mod. Phys. **57**, 287 (1985); G. Bergmann, Phys. Rep. **107**, 1 (1984).